

High-energy cosmic-ray nuclei from high- and low-luminosity gamma-ray bursts and implications for multi-messenger astronomy

Kohta Murase^{1,*}, Kunihito Ioka², Shigehiro Nagataki¹, and Takashi Nakamura³

¹*Yukawa Institute for Theoretical Physics, Kyoto University,
Oiwake-cho, Kitashirakawa, Sakyo-ku, Kyoto, 606-8502, Japan*

²*Theory Division, KEK (High Energy Accelerator Research Organization), 1-1 Oho, Tsukuba 305-0801, Japan*

³*Department of Physics, Kyoto University, Kyoto 606-8502, Japan*

(Dated: May 2)

Gamma-ray bursts (GRBs) are one of the candidates of ultra-high-energy ($\gtrsim 10^{18.5}$ eV) cosmic-ray (UHECR) sources. We investigate high-energy cosmic-ray acceleration including heavy nuclei in GRBs by using Geant 4, and discuss its various implications, taking both of high-luminosity (HL) and low-luminosity (LL) GRBs into account. This is because LL GRBs may also make a significant contribution to the observed UHECR flux if they form a distinct population. We show that not only protons but also heavier nuclei can be accelerated up to ultra-high energies in the internal, (external) reverse and forward shock models. We also show that the condition for ultra-high-energy heavy nuclei such as iron to survive is almost the same as that for \sim TeV gamma-rays to escape from the source and for high-energy neutrinos not to be much produced. The multi-messenger astronomy by neutrino and GeV-TeV gamma-ray telescopes such as IceCube and KM3Net, GLAST and MAGIC will be important to see whether GRBs can be accelerators of ultra-high-energy heavy nuclei. We also demonstrate expected spectra of high-energy neutrinos and gamma rays, and discuss their detectabilities. In addition, we discuss implications of the GRB-UHECR hypothesis. We point out, since the number densities of HL-GRBs and LL-GRBs are quite different, its determination by UHECR observations is also important.

PACS numbers: 95.85.Ry, 98.70.Rz, 25.20.-x, 14.60.Lm, 96.50.Pw, 98.70.Sa

I. INTRODUCTION

Gamma-ray bursts (GRBs) and supernovae (SNe) are the most powerful phenomena in the universe. The latter is believed to be the origin of high-energy cosmic rays below the knee $\approx 10^{15.5}$ eV. The former could also accelerate baryons up to high energies if the dissipation process is due to shock dissipation. Waxman, Milgrom & Usov and Vietri suggested that ultra-high-energy cosmic rays (UHECRs) are produced in GRBs [1, 2, 3]. Their suggestions were based on the two arguments. First is the requirement that relativistic outflows that make GRBs satisfy various conditions for baryons to be accelerated up to greater than 10^{20} eV. Second is that the energy generation rate required to account for the observed UHECR flux is comparable to the energy generation rate of observed gamma rays. The latter argument depends on the local GRB rate which is not well known observationally. If the local cosmological high-luminosity GRB (HL GRB) rate is not high enough, which may be suggested by recent observations [4, 5, 6], the required baryon loading becomes larger [7, 8, 9]. In addition, if the UHECR spectrum at the source is steeper than that with the spectral index $p \sim 2.0 - 2.3$ (as expected in the dip model, $p \sim 2.4 - 2.7$ [9, 10]), the total nonthermal cosmic-ray energy of GRBs, necessary for explaining the observed UHECR flux, would be larger than the radiation energy.

Despite such caveats, the GRB-UHECR hypothesis is still one of the most interesting possibilities for explanation of observed UHECRs, and it should be examined by future observations.

Recent observations have tentatively suggested that some GRBs may form a different class (see, e.g., [11, 12]). GRBs in this class are called low-luminosity GRBs (LL GRBs) or sub-energetic GRBs, which may be more common than HL GRBs. If this speculation is true, they can provide the significant energy as high-energy cosmic rays, neutrinos and gamma rays. Murase et al. [14] suggested that cosmic rays can be accelerated up to ultra-high energies ($\gtrsim 10^{18.5}$ eV) in LL GRBs, and LL GRBs may make an important contribution to the observed high-energy cosmic-ray flux and the diffuse neutrino background [14, 15]. Such LL GRBs were associated with energetic supernovae called hypernovae. As in cases of supernovae, cosmic-ray acceleration is expected at shocks formed by the high-velocity ejecta. In fact, if the magnetic field is sufficiently amplified, cosmic-rays can be accelerated up to very high energies, even to ultra-high energies. Wang et al. [16, 17] suggested that they could explain observed high-energy cosmic rays above the second knee, under the assumption that LL GRBs have the enough local rate higher than that of HL GRBs.

Recently UHECR observations have been greatly advanced thanks to (South) Pierre Auger Observatory (PAO). The UHECR spectrum deduced by PAO suggests the existence of the Greisen-Zatsepin-Kuz'min (GZK) cutoff energy which arises from the photomeson production process between UHECRs and cosmic microwave background (CMB) photons [18, 19]. In addition, PAO

*Electronic address: kmurase@yukawa.kyoto-u.ac.jp

recently revealed the anisotropy and rejected the isotropy of UHECRs above 60 EeV at 3σ level [20, 21]. It suggests that the distribution of UHECRs traces the matter distribution in the universe, although the origin of UHECRs is still unknown, that is, AGNs, GRBs and other possibilities remain (see the latest review for AGN and GRBs, e.g., [22]). Interestingly, the preliminary elongation rate data by PAO showed the break around $\sim 10^{18.35}$ eV [23]. Whether heavier nuclei becomes more important above this break as the energy increases (which seems conflict with HiRes data) is still under debate. It is because there are large uncertainties in hadronic interactions. On the other hand, recent results on UHECRs above 60 EeV by PAO may infer that protons are dominant sources [20, 21], although some authors dispute [24, 25]. Although the issue of the composition of UHECRs requires more and more studies, present data seem to allow the presence of significant fractions of ultra-high-energy (UHE) nuclei around the GZK cutoff energy, even if protons are dominant. Therefore, it is one of the important issues whether UHE nuclei can survive (i.e., UHE nuclei are not photodisintegrated and not depleted due to photomeson production during the dynamical time) in UHECR production sites.

In this paper, we study acceleration of high-energy cosmic-ray nuclei in very detail by exploiting numerical calculations, and discuss various implications for multimessenger astronomy. In Sec. II, we show that cosmic rays (protons and heavier nuclei) can be accelerated up to ultra-high energies in both of HL GRBs and LL GRBs. We consider the internal, (external) reverse and forward shock models.

If cosmic rays can be accelerated up to sufficiently high energies, high-energy neutrino production via the photomeson production process and/or pp reaction is unavoidable. Now, large neutrino detectors such as IceCube [26], KM3Net [27] are being constructed. ANITA [28] and PAO [29] can also detect very high-energy neutrinos. We have chances to see such high-energy neutrino signals, which are important as a probe of cosmic-ray acceleration, in the future. High-energy neutrino signals from HL GRBs were predicted in the context of the standard scenario of GRBs assuming that observed UHECRs come from GRBs [30, 31, 32, 33]. We also investigated the neutrino emission from GRBs in very detail [8, 14, 34, 35], and various predictions in the *Swift* era are summarized in Ref. [35]. In Sec. III, we demonstrate predicted neutrino spectra in some of our models and discuss implications for neutrino astronomy. We can see that neutrino signals highly suppressed when very heavy nuclei like iron can survive.

In Sec. IV, we also demonstrate gamma-ray spectra for some models when heavy nuclei can be accelerated up to ultra high energies and survive. In this section, we also show that very high-energy gamma rays with GeV-TeV energies can escape from the source under conditions where UHE heavy nuclei such as iron can survive. We can expect to detect high-energy gamma-ray

signals by upcoming Gamma-Ray Large Area Telescope (GLAST) and Cherenkov telescopes such as MAGIC as long as the source is nearby. Otherwise, high-energy gamma rays above \sim TeV are attenuated by the cosmic microwave/infrared background (CMB/CIB) photons ([38] and references there in).

In Appendix F, We also discuss various implications of the GRB-UHECR hypothesis (including the HLGRB-UHECR, LLGRB-UHECR and Hypernova-UHECR hypotheses) for UHECR astronomy. We see that the determination of the source number density of UHECR sources and extragalactic magnetic field (EGMF) strength is essential to test the hypothesis. In this paper, we shall hereafter use notations such as $Q_x = Q/10^x$ in cgs units.

II. ACCELERATION OF COSMIC-RAY NUCLEI IN GRBS

In the standard model of GRBs (for reviews, see, e.g., [39, 40, 41]), both of the prompt and afterglow emission are attributed to electromagnetic radiation from relativistic electrons accelerated in shocks. If relativistic outflows that make GRBs contain baryons, not only electrons but also protons (and heavier nuclei) will be accelerated. Although the detail of the acceleration mechanism is poorly known, we usually assume that the first-order Fermi acceleration mechanism works in GRBs, where the distribution of nonthermal cosmic rays is given by a power-law spectrum under the test-particle approximation (see reviews, e.g., [42]). Therefore, we have [35, 43]

$$\frac{dn_{\text{CR}}}{d\varepsilon_{\text{CR}}} = \frac{U_{\text{CR}}}{\int_{\varepsilon_{\text{CR}}^{\text{min}}}^{\varepsilon_{\text{CR}}^{\text{max}}} d\varepsilon_{\text{CR}} \varepsilon_{\text{CR}}^{-(p-1)}} \varepsilon_{\text{CR}}^{-p}, \quad (1)$$

where ε_{CR} is the energy of cosmic rays in the comoving frame, U_{CR} is the comoving cosmic-ray energy density, and p is the spectral index. As a shock becomes highly relativistic, the spectral index can deviate from values for non-relativistic shocks. In the diffusive small pitch-angle scattering regime, $p \simeq 2.2$ is obtained in the ultra-relativistic limit [44]. But the large-angle scattering can lead to harder spectral indices [45, 46]. For simplicity, we shall use $p = 2$ which is often expected for non-relativistic or mildly relativistic shocks with the compression ratio $r_c = 4$. The acceleration time scale is written as $t_{\text{acc}} = (\eta\varepsilon_N)/(ZeBc)$, which could be applied to the second-order Fermi acceleration mechanism when the Alfvén-wave speed is close to the light speed [47, 48, 49]. Here, ε_N is the cosmic-ray energy in the comoving frame and η is a pre-factor. For the most efficient acceleration, we can expect $\eta \sim (1 - 10)$ [47]. Throughout this paper $\eta = 1$ is used to obtain the *upper* limit of the maximum energy. Note that $\eta \sim 10$ would be a more realistic value, and the acceleration time scale with $\eta = 10$ is demonstrated in Ref. [8].

The maximum energy of cosmic-rays is determined by several criteria. One is derived from the requirement that

the Larmor radius of a particle should be smaller than the effective size of the acceleration region (the Hillas condition). In addition, the acceleration time scale should be smaller than the dynamical time scale t_{dyn} (which is essentially the same as the Hillas condition in our interested cases) and escape time scale t_{esc} . The maximum energy is also limited by the total cooling time scale $t_{\text{cool}}^{-1} \equiv t_{N\gamma}^{-1} + t_{\text{syn}}^{-1} + t_{\text{IC}}^{-1} + t_{\text{ad}}^{-1}$. Here, t_{syn} is the synchrotron cooling time scale, t_{IC} is the inverse-Compton cooling time scale and t_{ad} is the adiabatic cooling time scale. In cases of GRBs, we shall use $t_{\text{ad}} \approx t_{\text{dyn}}$ [30, 35, 50, 51]. $t_{N\gamma}$ is the photohadronic time scale which includes the photodisintegration, photomeson production and photopair production processes. For protons with sufficiently high energies, the photomeson production process is the most important, whose energy loss time scale is given by

$$t_{p\gamma}^{-1}(\varepsilon_p) = \frac{c}{2\gamma_p^2} \int_{\bar{\varepsilon}_{\text{th}}}^{\infty} d\bar{\varepsilon} \sigma_{p\gamma}(\bar{\varepsilon}) \kappa_p(\bar{\varepsilon}) \bar{\varepsilon} \int_{\bar{\varepsilon}/2\gamma_p}^{\infty} d\varepsilon \varepsilon^{-2} \frac{dn}{d\varepsilon}, \quad (2)$$

where $\bar{\varepsilon}$ is the photon energy in the rest frame of proton, γ_p is the proton's Lorentz factor, κ_p is the inelasticity of proton, and $\bar{\varepsilon}_{\text{th}} \approx 145$ MeV is the threshold photon energy for photomeson production. For heavier nuclei than proton, both of the photodisintegration and photomeson production processes are important, whose time scales are given by the similar expression to Eq. (2) [52]. In order to decide whether a kind of UHE nuclei can survive or not, we calculate the interaction time scale of photodisintegration and photomeson production by using the numerical simulation kit Geant4 [53], which includes the cross section data based on experimental data [54]. As seen later, it is important to use the accurate cross section in the high-energy range. Although we evaluate $t_{N\gamma}$ by numerical calculations, the simple analytic treatment is often useful. The most frequently used approximation for the photomeson production process is the Δ -resonance approximation (see, e.g., [30, 34]). The corresponding one for the photodisintegration process is the Giant-Dipole-Resonance (GDR) approximation. Similarly, we can apply it to the GDR approximation for a broken power-law photon spectrum. We have

$$t_{N\gamma}^{-1} \simeq \frac{U_\gamma}{5\varepsilon_{\text{ob}}^b} c \sigma_{\text{res}} \frac{\Delta\bar{\varepsilon}}{\bar{\varepsilon}_{\text{res}}} \begin{cases} (E_N/E_N^b)^{\beta-1} \\ (E_N/E_N^b)^{\alpha-1} \end{cases}, \quad (3)$$

where $E_N^b \simeq 0.5\bar{\varepsilon}_{\text{res}} m_N c^2 \Gamma^2 / \varepsilon_{\text{ob}}^b$, α is a photon index in lower energies while β in higher energies. The parameter regions for the upper and lower columns are $E_N < E_N^b$ and $E_N \geq E_N^b$, respectively. Here $\varepsilon_{\text{ob}}^b$ is the break energy measured by the observer in the local rest frame, and U_γ is the total photon energy density. For example, a Band function which reproduces spectra of the prompt emission, can be approximated by a broken power-law spectrum. Spectra of afterglows are also expressed by several segments of power-law spectra. The cross section at the resonant energy $\bar{\varepsilon}_{\text{res}}$ is expressed as σ_{res} . For GDR of nucleon, we use

$\sigma_{\text{GDR}} \sim 1.45 \times 10^{-27} \text{ cm}^2 A$, $\bar{\varepsilon}_{\text{GDR}} \sim 42.65 A^{-0.21} \text{ MeV}$ and $\Delta\bar{\varepsilon} \sim 8 \text{ MeV}$ [52, 55, 56, 57]. In the case of Δ -resonance of proton, we use $\sigma_\Delta \sim 4 \times 10^{-28} \text{ cm}^2$, $\bar{\varepsilon}_\Delta \sim 0.3 \text{ GeV}$, $\Delta\bar{\varepsilon} \sim 0.2 \text{ GeV}$ and $\kappa_p \sim 0.2$ [30, 34]. These approximations reproduce numerical results well except in high energies. In high energies, effects of non-GDR and/or non- Δ -resonance such as fragmentation and multi-pion production can become important, as seen later. This tendency can also be seen in $t_{p\gamma}$. As pointed out in Ref. [8], the effect of non- Δ -resonance such as multi-pion production becomes moderately important in high energies for spectra of the prompt emission where $\alpha \sim 1$.

For later discussions, let us introduce optical depths for photodisintegration of nuclei and photomeson production of protons, and define $f_{N\gamma} \equiv t_{\text{dyn}}/t_{N\gamma}$ and $f_{p\gamma} \equiv t_{\text{dyn}}/t_{p\gamma}$, respectively. These quantities express whether cosmic rays can survive in the source or not. For example, cosmic rays can survive from the photodisintegration and photomeson production processes if $f_{N\gamma} < 1$, while not if $f_{N\gamma} \geq 1$.

In the following subsections, we shall show that high-energy cosmic-ray nuclei can be produced in the internal and external shock models for HL and LL GRBs. GRBs may be even UHECR sources. In such cases, note that cosmic rays have to be accelerated above 10^{20} eV from observations of the highest energy events and the existence of the bump around the GZK cutoff energy. We shall allow for possibilities that observed highest UHECRs are UHE nuclei. It is because, although the arrival distribution and spectrum of UHECRs may be consistent with the proton model, some authors claimed that UHE nuclei are more important.

A. Internal Shock Model

The internal shock model is one of the most frequently discussed models in order to explain the prompt emission. Relativistic outflows make internal collisions, which lead to internal dissipation via shocks. The formed shocks will be mildly relativistic shocks, and charged particles will be accelerated at those collisionless shocks by some mechanism such as the Fermi acceleration mechanism. HL GRBs have luminosity $L_\gamma \sim 10^{51-52} \text{ ergs/s}$ and the observed peak energy $\varepsilon_{\text{ob}}^b \sim 10^{2.5} \text{ keV}$. The isotropic equivalent energy is $E_\gamma^{\text{iso}} \sim 10^{53} \text{ ergs}$ $L_{\gamma,52} [\delta t_{-1}/(1+z)] N_2$. Here δt is the variability time which can vary in the very wide range and N is the number of collisions. A typical collision radius will be expressed by commonly used relation, $r \approx 1.2 \times 10^{14} \Gamma_{2.5}^2 [\delta t/0.02(1+z)] \text{ cm}$. Of course, this radius has to be smaller than the deceleration radius where the afterglow begins. As discussed in Refs. [8, 36, 58], an internal collision radius is one of the most important quantities for the photomeson production. A collision radius $r \sim 10^{13-15} \text{ cm}$ is frequently assumed. The magnetic field is given by $B = 7.3 \times 10^4 \text{ G} \varepsilon_B^{1/2} (\Gamma_{\text{sh}}(\Gamma_{\text{sh}} - 1)/2)^{1/2} L_{\text{M},52}^{1/2} \Gamma_{2.5}^{-1} r_{14}^{-1}$.

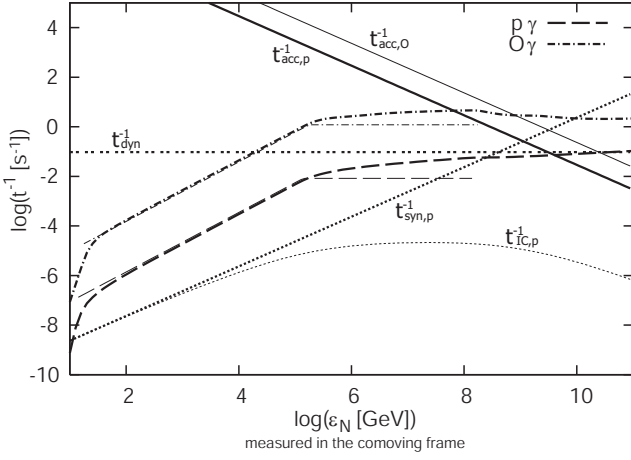


FIG. 1: The acceleration time scale and various cooling time scales of proton and oxygen in the internal shock model for HL GRBs. Energy and time scales are measured in the comoving frame of the outflow. Used parameters are $L_b = 10^{51.5} \text{ erg s}^{-1}$, $\epsilon_{\text{ob}}^b = 10^{2.5} \text{ keV}$, $\Gamma = 10^{2.5}$, $r = 10^{14} \text{ cm}$ and $\xi_B (\approx \epsilon_B/\epsilon_e) = 1$. Thick lines show numerical results on the photomeson and/or photodisintegration time scales. Thin lines show analytic results obtained by the resonance approximation. In the high energies, the effect of the non-resonant cross section becomes important. Note that this parameter set implies that a significant fraction of the energy carried by protons goes into neutrinos.

Here, L_M is the kinetic luminosity of outflows and Γ_{sh} is the relative Lorentz factor between two subshells. The typical width of subshells in the comoving frame l is typically given by $l = r/\Gamma$.

Next, let us evaluate maximum energies of cosmic rays by using several criteria. First, $t_{\text{acc}} = t_{\text{dyn}} \approx t_{\text{ad}}$ leads to

$$(1+z)E_{N,\text{ad}}^{\text{max}} = \frac{\Gamma Z e B l}{\eta} \simeq 6.9 \times 10^{20} \text{ eV } Z \eta^{-1} \epsilon_B^{1/2} \epsilon_e^{-1/2} \times \left[\frac{\Gamma_{\text{sh}}(\Gamma_{\text{sh}} - 1)}{2} \right]^{1/2} L_{\gamma,51}^{1/2} \Gamma_{2.5}^{-1}. \quad (4)$$

Note that the Hillas condition $r_L = l = r/\Gamma$ is already satisfied. Second, $t_{\text{acc}} = t_{\text{syn}}$ leads to

$$(1+z)E_{N,\text{syn}}^{\text{max}} = \sqrt{\frac{6\pi Z e}{Z^4 \sigma_T B \eta} \frac{\Gamma m_N^2 c^2}{m_e}} \simeq 4.2 \times 10^{20} \text{ eV } A^2 Z^{-3/2} \eta^{-1/2} \epsilon_B^{-1/4} \epsilon_e^{1/4} \times \left[\frac{\Gamma_{\text{sh}}(\Gamma_{\text{sh}} - 1)}{2} \right]^{-1/4} L_{\gamma,51}^{-1/4} \Gamma_{2.5}^{3/2} r_{14}^{1/2}. \quad (5)$$

Therefore, we can expect that cosmic rays can be accelerated up to ultra-high energies in the internal shock model of HL GRBs unless other cooling time scales such as $t_{p\gamma}$ are important.

The inverse Compton cooling time scale can be also calculated. For evaluation of t_{IC} , we need to give a

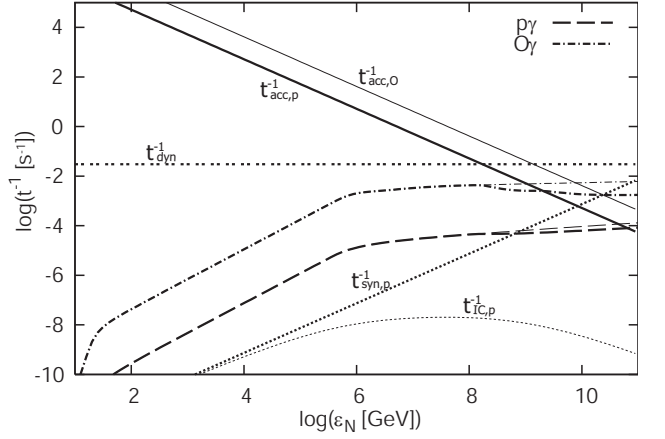


FIG. 2: The same as Fig. 1. But used parameters are $L_b = 10^{51} \text{ erg s}^{-1}$, $\epsilon_{\text{ob}}^b = 10^{2.5} \text{ keV}$, $\Gamma = 10^3$, $r = 10^{15} \text{ cm}$ and $\xi_B (\approx \epsilon_B/\epsilon_e) = 1$. Thick lines show numerical results with the synchrotron self-absorption cutoff 1 eV (in the comoving frame). Thin lines show analytic results without the low-energy cutoff for comparison. We can see that the effect of self-absorption is not so important for the maximum energy due to the effect of the non-resonant cross section in the high energies. Note that this parameter set allows for survival of UHE nuclei.

photon spectrum. The photon spectrum for the prompt emission is often approximated by the broken power-law as

$$\frac{dn}{d\varepsilon} = \frac{L_b e^{-(\varepsilon/\varepsilon^{\text{max}})}}{4\pi r^2 \Gamma^2 c (\varepsilon^b)^2} \begin{cases} (\varepsilon/\varepsilon^b)^{-\alpha} & (\text{for } \varepsilon^{\text{min}} \leq \varepsilon < \varepsilon^b) \\ (\varepsilon/\varepsilon^b)^{-\beta} & (\text{for } \varepsilon^b \leq \varepsilon \leq \varepsilon^{\text{max}}) \end{cases} \quad (6)$$

where L_b is the luminosity at the break energy measured by the observer in the local rest frame, ε^{min} is the minimum cutoff due to synchrotron self-absorption and ε^{max} is the maximum cutoff due to pair-creation in the comoving frame. In this paper, we set $\varepsilon^{\text{min}} = 1 \text{ eV}$ and $\varepsilon^{\text{max}} = 10 \text{ MeV}$. In this paper, we shall use $\alpha = 1$ and $\beta = 2.2$ as photon indices. Although t_{IC} is calculated, we can usually ignore this cooling time scale due to the Klein-Nishina suppression. Hence, $E_{N,\text{IC}}^{\text{max}}$ is usually larger than $E_{N,\text{syn}}^{\text{max}}$.

The effect of the photomeson production process of protons is investigated in detail in Ref. [8]. For details, see Refs. [8, 35] and references there in. At smaller collision radii, $t_{p\gamma}$ can be more important than other cooling time scales such as t_{syn} . UHE protons are not depleted only at sufficiently large radii. The cross section of photodisintegration is larger than that of photomeson production, so that survival of UHE nuclei is more difficult than survival of UHE protons. We evaluate the maximum energy due to photomeson production and/or photodisintegration, $E_{p,p\gamma}^{\text{max}}$ and/or $E_{N,N\gamma}^{\text{max}}$, from $t_{\text{acc}} = t_{p\gamma}$ and/or $t_{\text{acc}} = t_{N\gamma}$.

Our numerical results on various time scales in the internal shock model for HL GRBs are shown in Figs. 1 and 2. For calculations, we give the total photon energy

density U_γ by $U_\gamma = \int d\varepsilon \varepsilon \left(\frac{dn}{d\varepsilon}\right)$. The magnetic field is given by $U_B \equiv \xi_B U_\gamma \approx (\epsilon_B/\epsilon_e) U_\gamma$. Fig. 1 shows the result for $r = 10^{14}$ cm and $\Gamma = 10^{2.5}$. Thick lines show numerical results while thin lines show curves when we use resonance approximations. At sufficiently high energies, we can see that effects of the cross section in the non-resonance region become important. For this typical parameter set, we have the effective optical depth for the photomeson process $f_{p\gamma} \sim 0.3$. Hence, the efficient neutrino production occurs in this parameter set, which can lead to detectable neutrino signals [8, 30]. However, we cannot expect survival of UHE nuclei in such cases. Although they can be accelerated up to very high energies, UHE nuclei cannot survive in the sense that $f_{N\gamma} \gtrsim 1$.

Fig. 2 shows the result for $r = 10^{15}$ cm and $\Gamma = 10^3$. In this parameter set, we expect that UHECR nuclei can survive. Protons and oxygens can be accelerated up to $\sim 10^{20}$ eV and $\sim 10^{21}$ eV, respectively. This is just because the photon density becomes small enough at large radii. Note that we have the effective optical depth for the photomeson process $f_{p\gamma} \sim 10^{-3}$, which is a very small value. In this parameter set, although we can expect survival of UHE nuclei, the magnetic field is also expected to be rather weak as long as we use the conventional value $\xi_B = 1$. Here, we have $B \sim 5.8 \times 10^2$ G, which seems to be somewhat insufficient to explain the observed break energy by the optically thin synchrotron model. (Then, we expect $\varepsilon_{\text{ob}}^b \sim 12 \text{ keV} \Gamma_{2.5} (\Gamma_{\text{sh}} - 1)^2 \epsilon_e^2 g^2 f_e^{-2} B_3$, where $g = g(p) = (p - 2)/(p - 1)$ and p is the electron spectral index). But the detailed mechanism of the prompt emission has not been revealed yet [59], so that we do not consider this problem in this paper. In Fig. 2, we also show curves for spectra with the minimum cutoff energy (thick lines) and that without the cutoff (thin lines). Wang et al. [17] suggested that the effect of minimum cutoff energy (due to self-absorption) can increase the maximum energy of heavy nuclei. However, we see that the effect of self-absorption is not so important even at the highest energies due to the effect of the cross section in the non-resonance region, especially where the fragmentation process is important.

Next, let us consider LL GRBs such as GRB 060218 and GRB 980425. For example, GRB 060218 has low luminosity $L_\gamma \sim 10^{46-47}$ ergs/s, which is much smaller than that of usual HL-GRBs [60]. The duration time is $T \sim 3000$ s, and the isotropic equivalent energy is $E_\gamma^{\text{iso}} \sim 10^{50}$ ergs. The observed peak energy is $\varepsilon_{\text{ob}}^b \sim 5$ keV, hence this event is classified as a x-ray flash. Various interpretations for GRB 060218 exist. Several authors suggested the shock break-out model [61, 62]. Other authors argued that this event can be explained by the internal-external shock model [63, 64, 65]. In this paper, we adopt the conventional internal shock model following Toma et al. and we shall adopt the Lorentz factor $\Gamma \sim (5 - 10)$, which is suggested in Refs. [64, 65].

Fig. 3 shows one of our results for $r = 6 \times 10^{15}$ cm and $\Gamma = 10$, which correspond to $\delta t \sim 1000$ s when we use $r \approx 2\Gamma^2 c \delta t$. Results of other parameter sets are presented

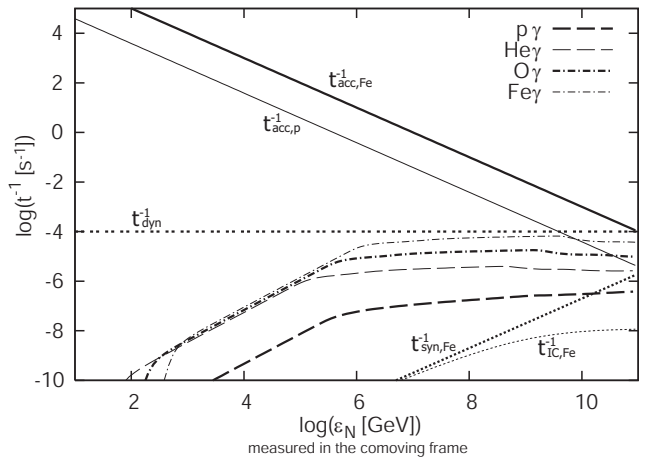


FIG. 3: The acceleration time scale and various cooling time scales of proton, helium, oxygen and iron in the internal shock model for LL GRBs. Energy and time scales are measured in the comoving frame of the outflow. Used parameters are $L_b = 1.5 \times 10^{46}$ erg s $^{-1}$, $\varepsilon_{\text{ob}}^b = 5$ keV, $\Gamma = 10$, $r = 6 \times 10^{15}$ cm (corresponding to $T = 10^3$ s) and $\xi_B (\approx \epsilon_B/\epsilon_e) = 1$. Note that this parameter set allows for survival of UHE nuclei.

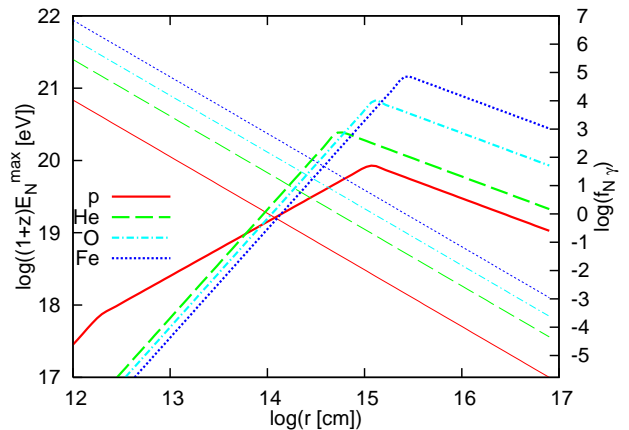


FIG. 4: The maximum energy of cosmic rays (thick lines) and the optical depth for photomeson production or photodisintegration (thin lines) as a function of the collision radius. Used parameters are $L_b = 1.5 \times 10^{46}$ erg s $^{-1}$, $\varepsilon_{\text{ob}}^b = 5$ keV, $\Gamma = 10$ and $\xi_B (\approx \epsilon_B/\epsilon_e) = 1$ for LL GRBs. The comoving shell width is set to $l = r/\Gamma$. Note that UHE nuclei can be produced in LL GRBs for $r \gtrsim 10^{15}$ cm. There, UHE nuclei can survive. At sufficiently large radii, E_N^{max} becomes $E_{N,\text{ad}}^{\text{max}}$.

in Appendix A. In this parameter set demonstrated in Fig. 3, we can expect that not only UHECRs can be produced but also accelerated UHE nuclei can survive. This is just because the photon density is small enough at large radii. Note that we have the effective optical depth for the photomeson process $f_{p\gamma} \sim 2 \times 10^{-3}$, which is a small value. In this parameter set, although we can expect survival of UHE nuclei, the magnetic field seems to be somewhat weak when we use the conventional value $\xi_B = 1$. In Fig. 3, Fe nuclei can be accelerated up to

$\sim 10^{21}$ eV, while protons only up to $\sim 10^{19.5}$ eV.

As noted before, one of the important parameters is a collision radius. Hence, we show maximum energies of proton and heavy nuclei E_N^{\max} as a function of a collision radius r in Fig. 4. In the same figure, $f_{p\gamma}$ and $f_{N\gamma}$ are shown. We can see that the maximum energy of proton is determined by the photomeson production at sufficiently small radii, but usually determined by the synchrotron cooling and adiabatic cooling processes at large radii ($r \gtrsim 10^{12.5}$ cm). The maximum energy of nucleon is usually determined by the photodisintegration and adiabatic cooling. Survival of UHE nuclei is possible only at $r \gtrsim 10^{15}$ cm in this parameter set.

B. Reverse Shock Model

The expanding fireball strikes the surrounding medium and will form a reverse shock and forward shock. The shocked ambient and ejecta materials are in pressure balance and are separated by a contact discontinuity. In the original standard model, the reverse shock is thought to be short-lived, which exists during the initial deceleration of the fireball. During this phase, optical/infrared flashes were expected. Indeed, some optical flashes can be interpreted as the reverse shock emission. However, recent observations have reported the tentative lack of bright optical/infrared flashes [66]. Although it is one of the open problems in the *Swift* era, we do not manage this problem in this paper. Recently, the modern version of the reverse shock model was developed to explain the shallow decay emission in the early afterglow phase [67, 68]. In such models, the plateau shape can be achieved by requiring the appropriate distribution of Lorentz factors of the ejecta and the suppression of the forward shock emission. For the reverse shock emission to emerge in the x-ray band, we can consider a number fraction of the shocked electrons that are injected into the acceleration process f_e^r to be smaller than the unity. In this paper, we shall consider cosmic-ray acceleration in the early afterglow phase under the reverse shock model developed for the shallow decay emission, and adopt the small f_e^r following Refs. [35, 67].

The cosmic-ray production in the reverse shock model was discussed in Refs. [3, 31, 32]. The more detailed study can be found in Ref. [35]. As demonstrated in these references, cosmic-ray acceleration up to ultra-high energies at a reverse shock of HL GRBs is possible. In this paper, let us demonstrate that UHE cosmic-ray production at a reverse shock of LL GRBs is also possible. First, $t_{\text{acc}} = t_{\text{dyn}} \approx t_{\text{ad}}$ leads to

$$(1+z)E_{N,\text{ad}}^{\max} = \frac{ZeB_{\times}^r r_{\times}}{\eta} \simeq 4.7 \times 10^{20} \text{ eV } Z\eta^{-1} \times \epsilon_B^{1/2} E_{\text{ej},50}^{3/8} n_2^{1/8} T_3^{1/8}, \quad (7)$$

where T is the duration time measured by the observer in the local rest frame. Here, we have assumed the thick

ejecta case, where the total ejecta thickness $\sim cT$ is larger than the shocked region at the crossing time $\sim r_{\times}/2\Gamma_0^2$. Here Γ_0 is the initial Lorentz factor. In the thin ejecta case, the corresponding expression can be derived easily. Second, $t_{\text{acc}} = t_{\text{syn}}$ leads to

$$(1+z)E_{N,\text{syn}}^{\max} = \sqrt{\frac{6\pi Ze}{Z^4 \sigma_T B_{\times}^r \eta} \frac{\Gamma m_N^2 c^2}{m_e}} \simeq 1.3 \times 10^{21} \text{ eV } A^2 Z^{-3/2} \eta^{-1/2} \times \epsilon_B^{-1/4} E_{\text{ej},50}^{-3/16} n_2^{-5/16} T_3^{-1/16}. \quad (8)$$

Therefore, we can expect that UHECR production at a reverse shock is possible not only for HL GRBs but also LL GRBs. Note that even protons could be accelerated above 10^{20} eV unless ϵ_B is too small.

Photon spectra in the reverse shock model can be calculated by exploiting the reverse-forward shock model. For example, in the slow cooling regime ($\epsilon^m < \epsilon^{sa} < \epsilon^c$), we obtain

$$\frac{dn}{d\epsilon} = n_{\epsilon,\text{max}} e^{-(\epsilon/\epsilon^{\text{max}})} \begin{cases} (\epsilon^{sa}/\epsilon^m)^{-\frac{p+1}{2}} (\epsilon^m/\epsilon^{sa})^{\frac{3}{2}} (\epsilon/\epsilon^m)^1 \\ (\epsilon^{sa}/\epsilon^m)^{-\frac{p+1}{2}} (\epsilon/\epsilon^{sa})^{\frac{3}{2}} \\ (\epsilon/\epsilon^m)^{-\frac{p+1}{2}} \\ (\epsilon^c/\epsilon^m)^{-\frac{p+1}{2}} (\epsilon/\epsilon^c)^{-\frac{p+2}{2}} \end{cases} \quad (9)$$

where [35, 43]

$$n_{\epsilon,\text{max}} = \frac{L_{\epsilon,\text{max}}}{4\pi r_{\times}^2 c \epsilon^n}. \quad (10)$$

Here $\epsilon^n \equiv \min[\epsilon^m, \epsilon^c]$, and ϵ^m , ϵ^c and ϵ^{sa} are the injection, cooling and self-absorption energy in the comoving frame, respectively. $L_{\epsilon,\text{max}}$ is the comoving specific luminosity per unit energy at the injection or cooling energy. From Eq. (9), we can calculate t_{IC} and $t_{N\gamma}$.

We show the numerical result of the reverse shock model for LL GRBs in Fig. 5. The used parameters are $E_{\text{ej}} = 2 \times 10^{51}$ ergs, $n = 10^2 \text{ cm}^{-3}$, $\epsilon_e^r = \epsilon_B^r = 0.1$, $f_e^r = 0.025$, $T = 3000$ s and the initial Lorentz factor $\Gamma_0 = 5$. As seen in Fig. 5, the UHECR production is possible, where protons and Fe nuclei can be accelerated up to $\sim 10^{20.2}$ eV. But we cannot expect survival of UHE nuclei in this parameter set due to the copious photon field. For UHE nuclei accelerated above 10^{20} eV to survive, for example, much smaller ϵ_e^r is needed. If we adopt such parameters, we can expect both UHE protons and nuclei in this model.

C. Forward Shock Model

The expanding fireball strikes the surrounding medium and will form a forward shock. The self-similar behavior after the deceleration time t_{dec} is described by the Blandford-McKee solution. The standard external shock model based on this solution can reproduce observations

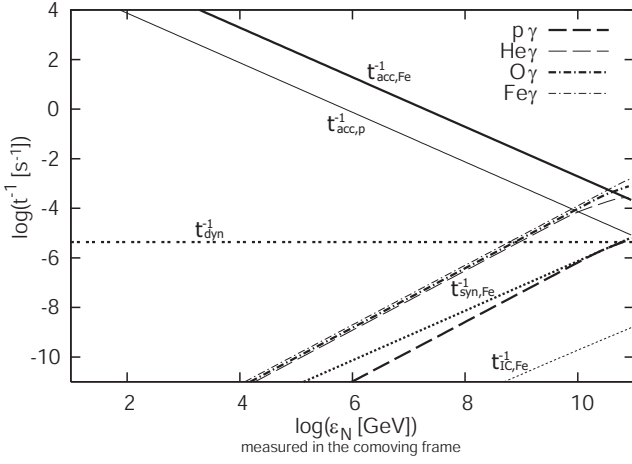


FIG. 5: The acceleration time scale and various cooling time scales of proton, helium, oxygen and iron in the reverse shock model for LL GRBs. Energy and time scales are measured in the comoving frame of the outflow. Used parameters are $E_{ej} = 2 \times 10^{51}$ ergs, $n = 10^2 \text{ cm}^{-3}$ (ISM), $\Gamma_0 = 5$, $T = 3 \times 10^3$ s, $\epsilon_B^r = 0.1$, $\epsilon_e^r = 0.1$, $f_e^r = 0.025$ and $p = 2.4$. Note that this parameter set does not allow for survival of UHE nuclei.

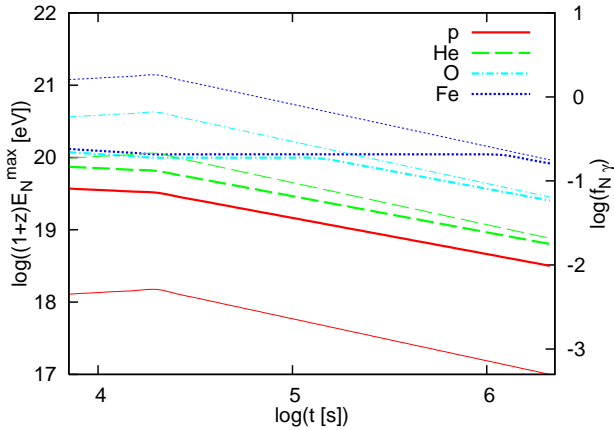


FIG. 6: The maximum energy of cosmic rays (thick lines) and the optical depth for photomeson production or photodisintegration at 10^{20} eV (thin lines) as a function of the time after the burst. Used parameters are $E_{ej} = 2 \times 10^{51}$ ergs, $n = 10^2 \text{ cm}^{-3}$ (ISM), $\epsilon_B = 0.01$, $\epsilon_e = 0.01$, $f_e = 0.1$ and $p = 2$. The jet-break time is set to $t_j = 2 \times 10^4$ s. Note that the deceleration time is $t_{dec} \simeq 8000$ s. UHE nuclei can be produced in a forward shock of LL GRBs. Survival of UHE nuclei becomes the most difficult at the jet-break time. At sufficiently late time, E_N^{\max} becomes $E_{N,ad}^{\max}$.

at the late time. Although the original forward shock model actually fails to explain the shallow decay emission, we consider the original forward shock model for simplicity. By exploiting the theory, we immediately have $\Gamma \propto t^{-\frac{3}{8}}$, $r \propto t^{\frac{1}{4}}$ and $B \propto t^{-\frac{3}{8}}$. By using them, we can derive the time-dependence of various quantities. Typical parameters for HL GRBs are $E_{ej} \sim 10^{52-53}$ ergs, $n = 1 \text{ cm}^{-3}$ (ISM), $\epsilon_B \sim 0.01$, $\epsilon_e \sim 0.1$ and $p \sim 2$. In

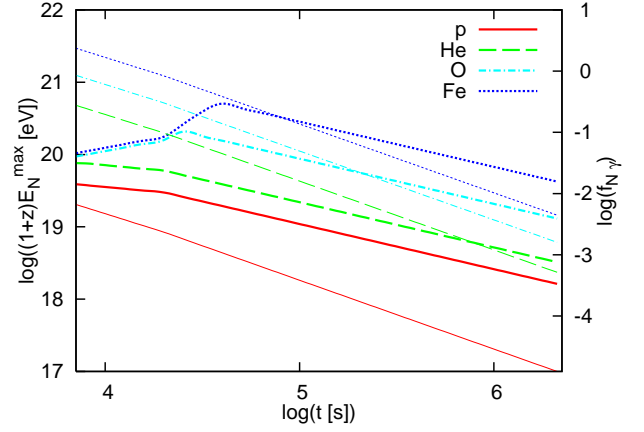


FIG. 7: The same as Fig. 6. But the wind-like circumburst medium is assumed ($A_* = 0.77$). UHE nuclei can be produced in a forward shock of LL GRBs. Survival of UHE nuclei becomes easier with time. At sufficiently late time, E_N^{\max} becomes $E_{N,ad}^{\max}$.

obtaining above parameters, all the electrons are often assumed to be accelerated. However, this may not be true. As Eichler & Waxman [69] discussed, only a fraction f_e of electrons may be accelerated, that is, f_e can be smaller than the unity. When we consider the small f_e , the kinetic energy of ejecta can be larger by $1/f_e$. Such small values of f_e will be tested by observations of polarization in the future [70].

Cosmic-ray acceleration and neutrino production in the forward shock model for HL GRBs were discussed in detail by Dermer [33, 50]. Hereafter, let us demonstrate UHECR production at a forward shock for parameters of LL GRBs. In this paper, we shall adopt $E_{ej} = 2 \times 10^{51}$ ergs, $n = 10^2 \text{ cm}^{-3}$ (ISM), $\epsilon_B = 0.01$, $\epsilon_e = 0.01$, $f_e = 0.1$ and $p = 2$. This parameter set is consistent with parameters obtained by Toma et al. [65] except that we use $f_e = 0.1$.

Next, let us estimate maximum energies of cosmic rays. First, the maximum energy determined from the condition $t_{acc} = t_{dyn} \approx t_{ad}$ is [35, 48, 49]

$$\begin{aligned} (1+z)E_{N,ad}^{\max} &= \frac{Ze\Gamma B^{\text{ISM}}r}{\eta} \\ &\simeq 7.1 \times 10^{14} \text{ eV } Z\eta^{-1} \\ &\times B_{-6}^{\text{ISM}} E_{ej,51}^{3/8} n_2^{-3/8} t_4^{-1/8}. \end{aligned} \quad (11)$$

Here $(1+z)t$ is the time after the prompt emission measured by the observer. When we use the conventional value of the ISM magnetic field, we cannot expect UHECR production at a forward shock of GRBs. However, the upstream magnetic field might be amplified significantly via some process, e.g., the non-resonant cosmic-ray streaming instability [33, 71] (but see also Ref. [72]). Instead, if the second-order Fermi acceleration works well [73], we could use the magnetic field in the downstream, which is likely to be amplified, as indicated

by observations. If the upstream and/or downstream magnetic fields are amplified up to near the equipartition value, $t_{\text{acc}} = t_{\text{dyn}} \approx t_{\text{ad}}$ leads to

$$(1+z)E_{N,\text{ad}}^{\text{max}} = ZeB^f r \eta^{-1} \simeq 2.7 \times 10^{20} \text{ eV } Z \eta^{-1} \\ \times \epsilon_B^{1/2} E_{\text{ej},51}^{3/8} n_2^{1/8} t_4^{-1/8}. \quad (12)$$

The maximum energy limited by synchrotron cooling is

$$(1+z)E_{N,\text{syn}}^{\text{max}} = \sqrt{\frac{6\pi Ze}{Z^4 \sigma_T B^f \eta} \frac{\Gamma m_N^2 c^2}{m_e}} \\ \simeq 2.5 \times 10^{20} \text{ eV } A^2 Z^{-3/2} \eta^{-1/2} \\ \times \epsilon_B^{-1/4} E_{\text{ej},51}^{1/16} n_2^{-5/16} t_4^{-3/16}. \quad (13)$$

From Eqs. (12) and (13), we can expect that UHECR production is also possible at a forward shock of LL GRBs.

A photon spectrum in the forward shock model can be also calculated from the theory. For example, in the slow cooling case ($\epsilon^{sa} < \epsilon^m < \epsilon^c$), we have

$$\frac{dn}{d\varepsilon} = \frac{L_{\varepsilon,\text{max}} e^{-(\varepsilon/\varepsilon^{\text{max}})}}{4\pi r^2 c \varepsilon^n} \begin{cases} (\varepsilon^{sa}/\varepsilon^m)^{-\frac{2}{3}} (\varepsilon/\varepsilon^{sa})^1 \\ (\varepsilon/\varepsilon^m)^{-\frac{2}{3}} \\ (\varepsilon/\varepsilon^m)^{-\frac{p+1}{2}} \\ (\varepsilon^c/\varepsilon^m)^{-\frac{p+1}{2}} (\varepsilon/\varepsilon^c)^{-\frac{p+2}{2}} \end{cases} \quad (14)$$

Here, $\varepsilon_{\text{ob}}^m = \Gamma \varepsilon^m \simeq 0.17 \text{ eV } g_{-1}^2 f_{e,-1}^{-2} \epsilon_{B,-2}^{1/2} \epsilon_{e,-1}^2 E_{\text{ej},51}^{1/2} t_4^{-3/2}$, $\varepsilon_{\text{ob}}^c = \Gamma \varepsilon^c \simeq 1.0 \text{ eV } \epsilon_{B,-2}^{-3/2} E_{\text{ej},51}^{-1/2} n_2^{-1} t_4^{-1/2}$ and $L_{\varepsilon_{\text{ob}},\text{max}} = \Gamma L_{\varepsilon,\text{max}} \simeq 7.8 \times 10^{56} \text{ s}^{-1} f_{e,-1} \epsilon_{B,-2}^{1/2} E_{\text{ej},51} n_2^{1/2} (\phi_p/0.6)$, where ϕ_p is an order-of-unity factor calculated by Wijers & Galama [74].

The photodisintegration and/or photomeson time scales are evaluated from Eq. (2). Here, let us estimate these time scales analytically in the slow cooling case by applying Eq. (3). After replacing ε^b with ε^c , resonance approximations give

$$t_{N\gamma}^{-1} \simeq g_{-1} (\phi_p/0.6) \epsilon_{e,-2} \epsilon_{B,-2}^{3/2} E_{\text{ej},51}^{7/8} n_2^{13/8} t_4^{-5/8} (E_N/E_N^b)^{1/2} \\ \times \begin{cases} 1.1 \times 10^{-8} \text{ s}^{-1} & (\text{for } \Delta\text{-resonance}) \\ 5.7 \times 10^{-8} A^{1.21} \text{ s}^{-1} & (\text{for GDR}) \end{cases} \quad (15)$$

The above expressions are obtained for $E_N > E_N^b = 0.5 \bar{\varepsilon}_{\text{res}} m_N c^2 \Gamma^2 / \varepsilon_{\text{ob}}^c$. Hence, we have $f_{N\gamma} \propto t^{\frac{1}{8}}$ and $E_{N,N\gamma}^{\text{max}} \propto t^{-\frac{1}{8}}$ for $E_N > E_N^b$. Of course, the time-dependence differs for $E_N < E_N^b$. In the ISM case, we can see that $f_{N\gamma}$ increases with time. Note that the temporal index of $f_{N\gamma}$ is different from that used in Wang et al. [17], because we consider $E_N \sim 10^{20} \text{ eV}$, where $E_N > E_N^b$ is typically expected rather than $E_N < E_N^b$ considered by them.

In the wind-medium case, we have $E_{N,\text{ad}}^{\text{max}} \propto t^{-\frac{1}{4}}$ and $E_{N,\text{syn}}^{\text{max}} \propto t^{\frac{1}{8}}$. Furthermore, we can derive $E_{N,N\gamma}^{\text{max}} \propto t^{\frac{1}{2}}$

and $f_{N\gamma} \propto t^{-1}$ for $E_N > E_N^b$. In the wind-medium case, we can see that $f_{N\gamma}$ decreases with time. It is because the ambient density drops as r^{-2} , which leads to rapid drop of the photon density with time.

In the light curve of afterglows of HL GRBs, we can often find the jet break around $t_j \sim 10^5 \text{ s}$. After the jet break, we have $r \propto t^0$, $\Gamma \propto t^{-1/2}$ and $B \propto t^{-1/2}$. Therefore, for example, we obtain $E_{N,\text{ad}}^{\text{max}} \propto t^{-\frac{1}{2}}$, $E_{N,\text{syn}}^{\text{max}} \propto t^{-\frac{1}{4}}$, $E_{N,N\gamma}^{\text{max}} \propto t^0$ and $f_{N\gamma} \propto t^{-\frac{1}{2}}$ for $E_N > E_N^b$ in the ISM case. After the jet break, the photon density will become smaller and smaller. Hence, we expect photodisintegration and photomeson production become less important. Similarly, we can obtain the time-dependence of various quantities for the wind-medium case. In both cases, the effect of the jet break makes survival of UHE nuclei easier. It has not been pointed out in previous studies.

Results in the forward shock model for LL GRBs are shown in Figs. 6 and 7. In Fig. 6, we show maximum energies of cosmic rays E_N^{max} and the optical depth for photodisintegration $f_{N\gamma}$ at $E_N = 10^{20} \text{ eV}$ as a function of time t . From this figure, we can expect UHE nuclei can be produced at a forward shock of LL GRBs. For heavy nuclei (O and Fe), the photodisintegration determines the maximum energy at the earlier time, but the adiabatic cooling becomes more important at the later time. For light nuclei, the adiabatic cooling is almost always the most important. Note that the jet-break effect can be important for survival of UHE nuclei, as expected. In fact, after the jet break, $f_{\text{Fe}\gamma}$ can decrease with time and become smaller than the unity.

In Fig. 7 we show the results for the wind-medium case. In this case, we also expect acceleration and survival of UHE nuclei. Since the photon density decreases with time, the maximum energy of heavy nuclei, which is determined by $E_{N,N\gamma}^{\text{max}}$, can increase until the adiabatic cooling becomes more important. As a result, UHE nuclei could be accelerated up to $\gtrsim 10^{20} \text{ eV}$ in this parameter set.

III. IMPLICATIONS FOR NEUTRINO ASTRONOMY

Sufficiently high-energy cosmic rays cannot avoid the photomeson production process, where the pion production threshold energy is 145 MeV. Generated pions, kaons and other mesons can produce high-energy neutrinos. Such high-energy neutrino signals, if detected, are very important as a direct probe of cosmic-ray acceleration. High-energy neutrino emission from accelerated protons at shocks was predicted by Waxman & Bahcall [30] in the internal shock model. Predictions were also done in the reverse-forward shock model [31, 32, 33]. Further predictions in the *Swift*-era are found in Refs. [14, 34, 35].

The important quantity for the neutrino flux originating from protons is the effective optical depth for the photomeson production process $f_{p\gamma}$, which also represents an energy fraction of protons carried by mesons, as long as

$f_{p\gamma} < 1$. When $f_{p\gamma} \gtrsim 1$, accelerated protons are depleted by photomeson production, which also means the efficient photomeson production. Such conditions are satisfied when internal shocks making the prompt emission occur at sufficiently small radii [8]. In addition, $f_{p\gamma} \gtrsim 1$ is also possible in the case of flares and late prompt emissions [34, 35].

On the other hand, when $f_{p\gamma} \lesssim 1$, high-energy protons can survive without complete depletion. Such conditions are satisfied when internal shocks making prompt emission occur at sufficiently large radii. In the reverse-forward shock model (with the ISM environment), $f_{p\gamma} \lesssim 1$ is usually expected except in the highest-energies. However, we still expect that a significant fraction of the non-thermal proton energy is released as neutrinos unless $f_{p\gamma}$ is too small [31, 33, 35].

In most previous works, all the cosmic rays are assumed to be protons. However, heavier nuclei may be entrained, which can also be accelerated up to ultra-high energies as shown in Sec. II. We can relate $f_{p\gamma}$ with $f_{N\gamma}$ as

$$\frac{f_{p\gamma}(E_N)}{(f_{N\gamma}(E_N)/A)} \simeq 0.2A^{-0.21} \begin{cases} E_N^{\beta-\alpha}(E_p^b)^{1-\beta}(E_N^b)^{\alpha-1} \\ (E_N^b/E_p^b)^{\alpha-1} \end{cases} \quad (16)$$

Here, the parameter regions for the upper and lower columns are $(E_N^b \leq) E_N < E_p^b$ and $E_N \geq E_p^b$, respectively. From Eq. (16), we can see that $f_{p\gamma}$ is small at radii where UHE heavy nuclei can survive, $f_{N\gamma} < 1$.

We can calculate neutrino spectra by using the same method as in Ref. [8]. When UHE heavy nuclei such as iron can survive, we easily expect that neutrino emission is not efficient from Eq. (16). For calculations, we assume that cosmic rays are all protons in cases where UHE irons cannot survive, while proton 75 % and iron 25 % in cases where UHE irons can survive. Although this cosmic-ray composition is just ad hoc, our results on neutrino spectra in GRBs do not depend on the composition so much, especially when UHE heavy nuclei survive, $f_{N\gamma} < 1$. The reason is as follows. The cross section of photomeson production for heavy nuclei is roughly expressed as $\sigma_{\text{meson}} \simeq A\sigma_{\Delta}$ (rather than $A^{2/3}\sigma_{\Delta}$ which is given in Ref. [17]), while the inelasticity around the Δ -resonance is around $0.2/A$. Hence, the energy loss time scales due to the photomeson production of heavy nuclei is written as $t_{\text{meson}} \approx t_{p\gamma}$. Hence, protons and irons generate similar neutrino fluence levels in cases of GRBs, as long as both are accelerated up to sufficiently high energies [75, 76].

As an example, let us show neutrino spectra expected in the prompt emission phase, which is the most frequently discussed since the prediction by Waxman & Bahcall [30]. We can evaluate $f_{p\gamma}$ and f_{meson} analytically by using the Δ -resonance approximation [30, 34]. For HL GRBs, we obtain

$$f_{p\gamma} \approx f_{\text{meson}} \simeq 0.3 \frac{L_{b,51.5}}{r_{14}\Gamma_{2.5}^2 \varepsilon_{\text{ob},316 \text{ keV}}^b} \begin{cases} (E_p/E_p^b)^{\beta-1} \\ (E_p/E_p^b)^{\alpha-1} \end{cases} \quad (17)$$

Here, the parameter regions for the upper and lower columns are $E_p < E_p^b$ and $E_p \geq E_p^b$, respectively, and we have multiplied a factor of ~ 2.5 due to the effect of the multi-pion production which is important for $\alpha \sim 1$ spectra [34]. For LL GRBs, we can apply the above expression [14] and have

$$f_{p\gamma} \approx f_{\text{meson}} \simeq 1.4 \times 10^{-3} \frac{L_{b,46.2}}{r_{15.8}\Gamma_{1.2}^2 \varepsilon_{\text{ob},5 \text{ keV}}^b} \begin{cases} (E_p/E_p^b)^{\beta-1} \\ (E_p/E_p^b)^{\alpha-1} \end{cases} \quad (18)$$

Here, the parameter regions for the upper and lower columns are $E_p < E_p^b$ and $E_p \geq E_p^b$, respectively. Our results are shown in Fig. 8. In fact, the above analytic estimations agree with numerical results. For example, let us consider parameter sets demonstrated in Fig. 1 for HL GRBs and Fig. 3 for LL GRBs. For the former set with the source redshift $z = 0.1$ ($E_{\gamma}^{\text{iso}} = 10^{53}$ ergs and $\xi_{\text{acc}} = 20$), we have $E_{\nu}^2 \phi_{\nu} \sim (1/4)f_{p\gamma} E_p^2 (dN_p^{\text{iso}}/dE_p)/(4\pi D^2) \sim 3 \times 10^{-4}$ ergcm $^{-2}$, which agrees with the thick solid line shown in Fig. 8. For the latter set with the source redshift $z = 0.005$ ($E_{\gamma}^{\text{iso}} = 10^{50}$ ergs and $\xi_{\text{acc}} = 10$), we have $E_{\nu}^2 \phi_{\nu} \sim (1/4)f_{p\gamma} E_p^2 (dN_p^{\text{iso}}/dE_p)/(4\pi D^2) \sim 7 \times 10^{-7}$ ergcm $^{-2}$, which also agrees with the thin dashed line shown in Fig. 8. Note that such low redshift bursts (at ~ 20 Mpc) have not been observed yet (e.g., ~ 40 Mpc for GRB 980425). But we may see such bursts if LL GRBs occur in e.g., Virgo cluster. The expected muon event rates by IceCube are also shown in the figure caption of Fig. 8. As stressed in the previous paragraph, survival of UHE heavy nuclei means that neutrino emission is inefficient, so that it would be difficult to expect detection of neutrino signals by near-future neutrino telescopes such as IceCube.

Since it is difficult to see neutrino signals from one GRB event, we may need to see many neutrino events as the cumulative neutrino background. As we can see from Eqs. (C1) and (C2), the cumulative neutrino flux can be estimated from $\min[1, f_{p\gamma}]$ and a given cosmology (see Appendix C). We typically expect $\min[1, f_{p\gamma}] \sim (0.01 - 1)$, for example, in the internal shock model for HL GRBs with $\Gamma \lesssim 10^{2.5}$ and $r \lesssim 10^{15.5}$ cm. Smaller values are possible only at larger radii and/or for larger Lorentz factors. Survival of UHE heavy nuclei such as iron requires such relatively extreme parameter sets, which leads to $f_{p\gamma} \sim 10^{-3}$. As a result, the expected cumulative neutrino flux under the GRB-UHECR hypothesis is $E_{\nu}^2 \Phi_{\nu} \sim 10^{-8}$ GeVcm $^{-2}$ s $^{-1}$ sr $^{-1}$ for the parameter set demonstrated in Fig. 1, while $E_{\nu}^2 \Phi_{\nu} \sim 3 \times 10^{-11}$ GeVcm $^{-2}$ s $^{-1}$ sr $^{-1}$ for the parameter set demonstrated in Fig. 2. The corresponding muon event rates by IceCube are $N_{\mu} \sim 50$ events/yr and $N_{\mu} \sim 0.05$ events/yr, respectively. Since the neutrino flux from nuclei is very similar to that from protons when accelerated heavy nuclei survive, we can use results obtained in Murase & Nagataki for mixed composition cases where UHE nuclei can survive. The detailed numerical calculations on the cumulative neutrino background are found

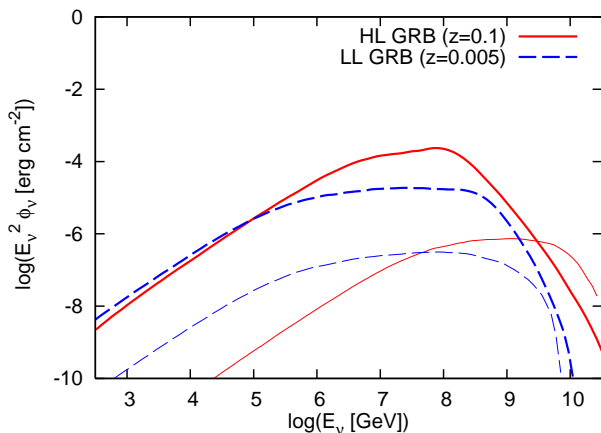


FIG. 8: Energy fluences of neutrinos from one nearby GRB event. Solid lines and dashed lines show HL GRB with $E_{\gamma}^{\text{iso}} = 10^{53}$ ergs at $z = 0.1$ and LL GRB with $E_{\gamma}^{\text{iso}} = 10^{50}$ ergs at $z = 0.005$, respectively. A thick solid line shows the HL-GRB neutrino spectrum for $r = 10^{14}$ cm and $\Gamma = 10^{2.5}$ where heavy nuclei cannot survive, while a thin solid line shows the HL-GRB neutrino spectrum for $r = 10^{15}$ cm and $\Gamma = 10^3$ where heavy nuclei can survive (see Figs. 1 and 2). A thick dashed line shows the LL-GRB neutrino spectrum for $r = 9 \times 10^{14}$ cm and $\Gamma = 10$ where heavy nuclei cannot survive, while a thin dashed line shows the LL-GRB neutrino spectrum for $r = 6 \times 10^{15}$ cm and $\Gamma = 10$ where heavy nuclei can survive (see Figs. 3 and 10). The cosmic-ray composition with proton 100 % is assumed for thick lines, while proton 75 % and iron 25 % for thin lines. The nonthermal baryon loading factors $\xi_{\text{acc}} \equiv U_{\text{CR}}/U_{\gamma}$ are set to 20 for HL GRBs and 10 for LL GRBs, respectively (see Appendix B). We also use $\xi_B \equiv U_B/U_{\gamma} = 1$. Expected muon event rates by IceCube are $N_{\mu} \sim 1$ event for the thick solid line, $N_{\mu} \sim 0.001$ events for the thin solid line, $N_{\mu} \sim 0.2$ events for the thick dashed line and $N_{\mu} \sim 0.002$ events for the thin dashed line.

in Refs. [8, 14, 34, 35]. In Ref. [8], neutrino spectra are shown for various collision radii and it is useful to compare set A and set B in Figs. 15-17, for example. So far we have considered the internal shock model. For other models, see Appendixes D and E.

IV. IMPLICATIONS FOR GAMMA-RAY ASTRONOMY

Not only neutrinos but also high-energy gamma rays originating from cosmic rays (cosmic-ray synchrotron radiation), neutral pions, and muons, electrons and positrons from charged pions will be produced. However, such high-energy gamma rays generally suffer from the internal attenuation processes, especially in the internal shock model, as discussed in many papers (see, e.g., [36] and references there in). The copious photon field also plays an important role on the efficient photomeson production, so that we cannot expect that GRBs are bright in \sim TeV gamma rays when bright in neutrinos (see Refs.

[37, 77] and references there in). In other words, when $f_{p\gamma}$ becomes small enough, we can expect that the optical depth for pair-creation $f_{\gamma\gamma}$ becomes smaller than the unity (hence high-energy gamma rays from far sources will be attenuated by CMB/CIB photons rather than seed photons in the source). As seen in the previous section, when UHE heavy nuclei can survive, $f_{p\gamma}$ is much smaller than the unity. Therefore, we may expect escape of very high-energy gamma rays from the source when UHE heavy nuclei can survive. Such high-energy gamma-ray signals are useful as signatures of UHECR acceleration, so that they are important although the distinction between hadronic and leptonic components is not so easy in general. Note that, when $f_{p\gamma}$ is large enough, one may not expect high-energy gamma rays due to internal attenuation. But proton-induced cascaded gamma-ray signals could be seen, e.g., when the baryon loading factor is large enough $\xi_{\text{acc}} \gg 10$ [77, 78]. Hence, observations of high-energy gamma rays are still important as a probe of the UHECR acceleration. See also [79].

As an example, let us consider the internal shock model with $\alpha = 1$ and $\beta = 2.2$. The optical depth for pair-creation process (which is usually relevant for escape of high-energy gamma rays) can be approximately written as $f_{\gamma\gamma}(\varepsilon_{\text{ob}}) \simeq 0.12\sigma_T\tilde{\varepsilon}(dn/d\varepsilon)_{\varepsilon}l$ [36, 80]. Here $\tilde{\varepsilon}$ is defined as $(m_e c^2)^2/\varepsilon$. When $\alpha \sim 1$, the optical depth for pair-creation $f_{\gamma\gamma}$ roughly reaches the maximum value at $\sim \tilde{\varepsilon}_{\text{ob}}^b = \Gamma^2(m_e c^2)^2/\varepsilon_{\text{ob}}^b$. (Note that, in fact, $f_{\gamma\gamma}(\varepsilon_{\text{ob}})$ increases logarithmically above $\sim \varepsilon_{\text{ob}}^b$ while decreases above $\tilde{\varepsilon}_{\text{ob}}^{sa}$.) On the other hand, as seen in the previous section, $f_{N\gamma}$ is also determined by the photon field. Therefore, we can relate the two quantities. Note that, in cases of $\alpha \sim 1$, the numerically calculated $f_{N\gamma}$ will be effectively larger than that evaluated analytically by using Eq. (3) by a factor of ~ 3 . Taking into account this factor, $f_{\gamma\gamma}$ at ε_{ob} can be written as

$$\frac{f_{\gamma\gamma}(\varepsilon_{\text{ob}})}{f_{N\gamma}(E_N)} \simeq 0.95 \left(\frac{A}{56}\right)^{-1.21} \begin{cases} (\varepsilon_{\text{ob}}/\tilde{\varepsilon}_{\text{ob}}^b)^{1.2} \\ 1 \end{cases} \quad (19)$$

Here, the parameter regions for the upper and lower columns are $\varepsilon_{\text{ob}} < \tilde{\varepsilon}_{\text{ob}}^b$ and $\varepsilon_{\text{ob}} \geq \tilde{\varepsilon}_{\text{ob}}^b$, respectively. From the above expressions, we can expect that the cosmic-ray source where UHE irons can survive ($f_{\text{Fe}\gamma} \lesssim 1$) is almost completely thin for pair-creation ($f_{\gamma\gamma} \lesssim 1$). This implies that very high-energy gamma rays are expected in the prompt phase, if UHE irons can be accelerated at internal shocks and survive. In Fig. 9, we demonstrate gamma-ray spectra from one HL GRB at $z = 0.1$ and LL GRB at $z = 0.005$. Gamma-ray spectra given by Eq. (6) and originating from cosmic-ray synchrotron radiation are shown. The former usually attributes to synchrotron (or jitter) radiation from accelerated electrons. The latter component should exist if cosmic rays can be accelerated to ultra high energies. Very high-energy gamma rays can be also produced via synchrotron self-inverse Compton scattering, which should contaminate the cosmic-ray synchrotron component. Whether

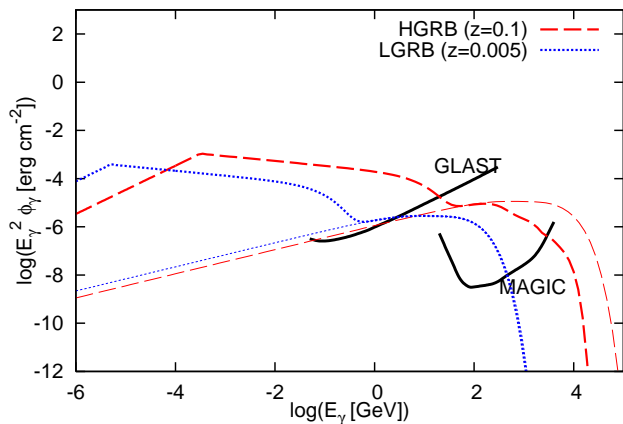


FIG. 9: Energy fluences of gamma rays from one nearby GRB event. Dashed and dotted lines show HL GRB with $E_{\gamma}^{\text{iso}} = 10^{53}$ ergs at $z = 0.1$ and LL GRB with $E_{\gamma}^{\text{iso}} = 10^{50}$ ergs at $z = 0.005$, respectively. A thick dashed line shows the HL-GRB gamma-ray spectrum for $r = 10^{15}$ cm and $\Gamma = 10^3$ where heavy nuclei can survive (see Fig. 2). A thin dashed line shows the only cosmic-ray synchrotron component from one HL GRB without attenuation by the CMB and CIB. A thick dotted line shows the LL-GRB gamma-ray spectrum for $r = 6 \times 10^{15}$ cm and $\Gamma = 10$ where heavy nuclei can survive (see Fig. 3). A thin dotted line shows the only cosmic-ray synchrotron component from one LL GRB without attenuation by the CMB and CIB. Note that synchrotron self-inverse Compton components by accelerated electrons are not shown. We assume the cosmic-ray composition with proton 75 % and iron 25 %. $\xi_{\text{acc}} \equiv U_{\text{CR}}/U_{\gamma}$ and $\xi_B \equiv U_B/U_{\gamma}$ are set to 20 and 10 for the HL GRB case, while 10 and 1 for the LL GRB case (see Appendix B). We use the low-IR model for the CIB, which is presented by Kneiske et al. [81]. Fluence sensitivity curves of GLAST and MAGIC are also shown [82, 83].

such a synchrotron self-inverse Compton component exists or not, we can expect to detect high-energy gamma-rays by GLAST and/or MAGIC in the future, as long as accelerated UHE heavy nuclei survive and GRBs occur at $z \lesssim 1$ for HL GRBs and $z \lesssim 0.05$ for LL GRBs, from Fig. 9.

Gamma rays can be produced by not only cosmic-ray synchrotron radiation but also neutral pions, charged pions, muons and electron-positron pairs generated via photomeson production. Gamma rays originating from photomeson production have very high energies (e.g., $\gtrsim 10$ PeV for gamma rays coming from neutral pion decay). Such gamma rays cannot avoid attenuation by the CIB, CMB and cosmic radio background. In fact, the mean free path of 10 PeV photons against pair-creation by the CMB photons is ~ 10 kpc, so that we cannot expect to detect such gamma rays directly [22]. Secondary electron-positron pairs generated by pair-creation are still energetic and up-scatter cosmic background photons. These boosted photons can create pairs if they are still energetic, and the process repeats itself until the energy of degraded photons is in the 1 – 10 TeV range

[84, 85]. The mean free path of these regenerated 1 – 10 TeV photons is longer than 100 Mpc, and they can reach the Earth. Whether the detection of these secondary gamma rays is possible or not depends strongly on the intergalactic magnetic field strength [86]. As it is large, the expected secondary flux becomes highly suppressed (see, e.g., [38] and references there in). It is because the duration of secondary emission becomes long and the emission becomes isotropic (for $\gtrsim 10^{-16}$ G). Only when the intergalactic magnetic field is very weak, which can be expected in the void region rather than the structured region, the secondary emission can be detected. Even in such cases, we expect that the secondary flux is subdominant compared to the primary flux for parameter sets in Fig. 9. In fact, the expected fluence originating from gamma rays from photomeson production can be estimated as $E_{\gamma}^2 \phi_{\gamma} \sim 10^{-7}$ ergcm $^{-2}$ for HL GRB and $E_{\gamma}^2 \phi_{\gamma} \sim 10^{-8}$ ergcm $^{-2}$, respectively [84, 85]. In addition, the secondary fluence from cosmic-ray synchrotron emission (estimated by using the same method presented in Ref. [38]) is smaller than the primary one. Therefore, we omit spectra of secondary delayed emission in this paper [87]. Note that the diffuse gamma-ray background from GRBs will be much smaller than the EGRET limit, which is expected to be $E_{\gamma}^2 \Phi_{\gamma} \lesssim 10^{-8}$ GeV cm $^{-2}$ s $^{-1}$ sr $^{-1}$ [38, 89]. So far we have considered the internal shock model. For other models, see Appendixes D and E.

V. SUMMARY AND DISCUSSION

In this paper, we have shown that not only protons but also heavy nuclei can be accelerated up to ultra-high energies in both of HL GRBs and LL GRBs. We exploit the internal shock model, (external) reverse shock model and forward shock model. We have also discussed various implications for neutrino, gamma-ray and UHECR astronomy. Especially, we have studied cosmic-ray acceleration in LL GRBs which may play an important role as high-energy cosmic-ray sources.

Let us summarize this paper below. First, we have shown that UHECR nuclei can be produced in both of HL GRBs and LL GRBs.

(A1) In the internal shock model, UHE protons and heavier nuclei can be produced in both of HL GRBs and LL GRBs. However, the allowed parameter range is limited. At smaller radii, most of the UHE nuclei are depleted, and a significant fraction of the nonthermal cosmic-ray energy is transferred into neutrinos. On the other hand, survival of UHE nuclei is possible only at large radii and/or for large Lorentz factors. Typically, relatively large radii $r \gtrsim 10^{15}$ cm will be required. For HL GRBs with $L_b \sim 10^{51-52}$ ergs $^{-1}$, both of protons and heavier nuclei can be accelerated up to ultra-high energies above 10^{20} eV. For LL GRBs with $L_b \sim 10^{46-47}$ ergs $^{-1}$, heavy nuclei can be accelerated above 10^{20} eV, while proton acceleration above such high energies may be difficult. In addition, we have shown that the effect of syn-

chrotron self-absorption suggested by Wang et al. [17] is not so important due to the cross section in the non-resonant region.

(A2) In the (external) reverse shock model, UHE nuclei can be produced in both of HL GRBs and LL GRBs. Not only heavy nuclei but also protons achieve ultra-high energies above $\sim 10^{20}$ eV. Whether heavy nuclei can survive or not depends on various parameters, and the sufficiently low photon density is required for survival. That is, small E_{ej} , ϵ_e , ϵ_B and n are needed. Conversely, if values of these parameters are large enough, in which optical/infrared are often expected, survival of UHE nuclei is impossible. Note that UHE nuclei produced at internal shocks could be photodisintegrated by photons generated at the reverse shock, when the ejecta is in the thick ejecta regime. Hence, we could not expect survival of UHE nuclei, when we see strong optical/infrared flashes.

(A3) In the (external) forward shock model, not only heavy nuclei but also protons can achieve ultra high energies above $\sim 10^{20}$ eV in both of HL GRBs and LL GRBs. When the photon density is sufficiently low, survival of UHE nuclei is possible. The relevant parameters $f_{N\gamma}$ and maximum energy E_N^{max} depend on time. In the ISM case, $f_{N\gamma}$ monotonically increases with time before the jet break occurs. On the other hand, in the wind-medium case, $f_{N\gamma}$ monotonically decreases with time. We have shown that the jet-break effect can be important for survival of UHE nuclei, which was not pointed out previously. After the jet break, the photon density decreases, so that survival of UHE nuclei becomes easier.

In the internal shock model and reverse shock model, we have to assume that heavy nuclei are contained in relativistic outflows of GRBs. It is natural to consider that only light elements can be synthesized in such a highly relativistic outflows due to the high photon to baryon ratio [90, 91]. However, there may be possibility that such an outflow is contaminated with heavy nuclei that are produced by explosive nucleosynthesis [92, 93, 94, 95]. Also, such heavy nuclei can be entrained from the stellar surroundings due to Kelvin-Helmholtz instabilities and/or oblique shocks [96]. Whether entrained heavy nuclei can survive or not is the issue that should be carefully examined. On the other hand, in the forward shock model and supernova model, heavy nuclei will be supplied by the swept material. They could come from the stellar wind of the progenitor star, e.g., the Wolf-Rayet star.

(B) Neutrino astronomy is useful as a direct probe of cosmic-ray acceleration, although the detection is not so easy. High-energy neutrinos from GRBs have been predicted in various contexts. If detected, we can obtain very useful information on cosmic-ray acceleration in GRBs. In this paper, we have calculated neutrino spectra from HL GRBs and LL GRBs in the internal shock model. We have shown that the neutrino detection by near-future telescopes such as IceCube and KM3Net would be difficult, when acceleration and survival of UHE heavy nuclei (such as iron) are possible. In the internal shock model,

for example, we can expect $N_\mu \sim 1$ event from one GRB at $z = 0.1$ and $N_\mu \sim 50$ events/yr as the cumulative background for one of the typical parameter sets (where UHE heavy nuclei cannot survive), with large baryon loading factors required in the GRB-UHECR hypothesis. On the other hand, survival of UHE heavy nuclei leads to much smaller neutrino fluxes, as we have demonstrated. Hence, second generation neutrino telescopes would be needed for neutrino detection in the latter case, although observations by IceCube and KM3Net would be useful to constrain the GRB-UHECR hypothesis.

(C) We can also expect high-energy gamma-ray emissions (including leptonic and hadronic gamma rays) from GRBs as well as high-energy neutrinos. We have shown that high-energy gamma rays above TeV can escape from the source, when UHE heavy nuclei (such as iron) can survive. As an example, we have calculated and evaluated gamma rays coming from accelerated cosmic rays in the internal shock model. If the source is nearby, we have seen that high-energy gamma rays from cosmic-ray synchrotron radiation would be detected by GLAST, MAGIC and VERITAS, with large baryon loading factors required in the GRB-UHECR hypothesis. (However, we should keep in mind that the synchrotron self-inverse Compton radiation by accelerated electrons could be more important.) Hence, the high-energy gamma-ray detection will also be one of the important clues to testing the GRB-UHECR hypothesis. When the intrinsic pair-creation optical depth becomes high enough (which infers UHE nuclei cannot survive), escape of TeV gamma rays becomes impossible and the intrinsic pair-creation cutoff should exist. But we may still find signatures of UHECR acceleration [78], although we cannot expect survival of UHE heavy nuclei in GRBs.

In this paper, we have demonstrated spectra of high-energy neutrinos and gamma rays, which are expected if GRBs are UHECR accelerators, by using detailed numerical calculations. We have also discussed detectabilities of such high-energy emission in the near future. Not only neutrino and gamma-ray astronomy but also UHECR astronomy are becoming important to test the GRB-UHECR hypothesis. In Appendix F, we have discussed implications of the GRB-UHECR hypothesis for UHECR astronomy by exploiting qualitative arguments. Future observations of UHECRs may allow us to distinguish between bursting sources and steady sources. If UHECR sources are bursting sources such as GRBs, we expect to obtain information on the effective EGMF and source number density by using the observed anisotropy of UHECRs. If we can, we could constrain the local bursting rate, for example, which may allow us to distinguish between HL GRBs and LL GRBs.

When we are preparing this work, we found that Wang et al. [17] studied acceleration of UHE nuclei in GRBs independently. In this paper, we have studied in more detail by making use of the detailed cross section and spectra of afterglows, and calculate spectra of high-energy neutrinos and gamma rays. Furthermore, we have also

studied cosmic-ray acceleration in LL GRBs.

Acknowledgments

KM thanks C. Dermer because he made very profitable comments at the conference TAUP2007 on September, 2007. KM also thanks the referee, R. Blandford, X.Y. Wang, Y.Z. Fan, K. Asano, S. Inoue and H. Takami. We thank R. Yamazaki and K. Toma for helpful comments. The work of KM is supported by a Grant-in-Aid for JSPS. The work of KI is supported by Grants-in-Aid for Scientific Research of the Japanese Ministry of Education, Culture, Sports, Science, and Technology 18740147 and 19047004. The work of SN is supported by Grants-in-Aid for Scientific Research of the Japanese Ministry of Education, Culture, Sports, Science, and Technology 19104006, 19740139, 19047004. The work of TN is supported by Grants-in-Aid for Scientific Research of the Japanese Ministry of Education, Culture, Sports, Science, and Technology 19047004. The work of us is supported by a Grant-in-Aid for the 21st Century Center of Excellence ‘‘Center for Diversity and University in Physics’’ from the Ministry of Education, Culture, Sports, Science and Technology of Japan.

APPENDIX A: COSMIC-RAY ACCELERATION AT INTERNAL SHOCKS OF LL GRBS

In this section, we discuss acceleration and survival of UHE nuclei in the internal shock model of LL GRBs. We think that it is important to demonstrate whether acceleration and survival of UHE nuclei are possible or

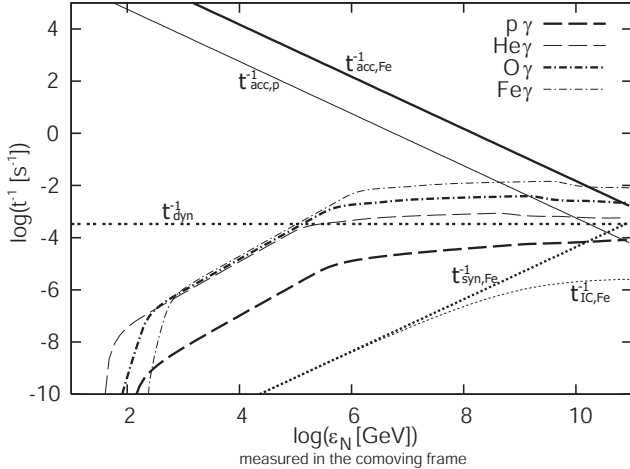


FIG. 10: The same as Fig. 3. But used parameters are $L_b = 10^{47} \text{ erg s}^{-1}$, $\epsilon_{\text{ob}}^b = 5 \text{ keV}$, $\Gamma = 10$, $r = 9 \times 10^{14} \text{ cm}$ (corresponding to $\delta t/(1+z) = 150 \text{ s}$) and $\xi_B (\approx \epsilon_B/\epsilon_e) = 1$. Note that this parameter set is the same one as used in Ref. [14] and it implies that a moderate fraction of the energy carried by protons goes into neutrinos.

not, because a kind of fine tuning is necessary. In fact, the parameter range such that acceleration and survival of UHE nuclei is possible (see Fig. 3) is rather limited, and we can more easily find parameter sets such that acceleration or survival of UHE nuclei is impossible. Note that collision radii of LL GRBs are largely uncertain. We can expect $r \sim 10^{15-16} \text{ cm}$, which implies the time scale $\delta t \sim 10^{2-3} \text{ s}$ [14, 15, 65]. In fact, the observed light curve of GRB 060218 is relatively simple and smooth. However, the collision radius may be much smaller as suggested in Ref. [64].

As in cases of HL GRBs, we can evaluate the maximum energies as (see also Ref. [14])

$$(1+z)E_{N,\text{ad}}^{\text{max}} = \frac{\Gamma Z e B l}{\eta} \simeq 2.2 \times 10^{20} \text{ eV } Z \eta^{-1} \epsilon_B^{1/2} \epsilon_e^{-1/2} \times \left[\frac{\Gamma_{\text{sh}}(\Gamma_{\text{sh}} - 1)}{2} \right]^{1/2} L_{\gamma,47}^{1/2} \Gamma_1^{-1} \quad (\text{A1})$$

and

$$(1+z)E_{N,\text{syn}}^{\text{max}} = \sqrt{\frac{6\pi Z e}{Z^4 \sigma_T B \eta} \frac{\Gamma m_N^2 c^2}{m_e}} \simeq 7.4 \times 10^{19} \text{ eV } A^2 Z^{-3/2} \eta^{-1/2} \epsilon_B^{-1/4} \epsilon_e^{1/4} \times \left[\frac{\Gamma_{\text{sh}}(\Gamma_{\text{sh}} - 1)}{2} \right]^{-1/4} L_{\gamma,47}^{-1/4} \Gamma_1^{3/2} r_{15}^{1/2}. \quad (\text{A2})$$

Therefore, we expect that LL GRBs also can produce UHECRs, especially that UHE nuclei can be accelerated above 10^{20} eV . These two conditions (Eqs. (A1) and (A2)) equivalently lead to inequalities (ignoring the term

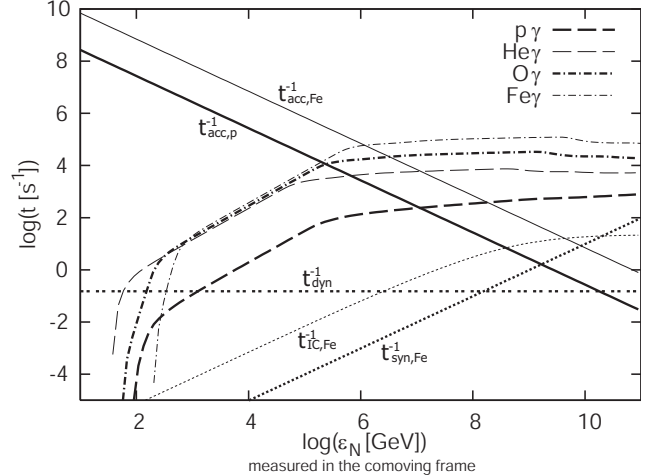


FIG. 11: The same as Fig. 3. But used parameters are $L_b = 10^{47} \text{ erg s}^{-1}$, $\epsilon_{\text{ob}}^b = 5 \text{ keV}$, $\Gamma = 5$, $r = 7 \times 10^{12} \text{ cm}$, $l = 10^{11} \text{ cm}$ and $\xi_B (\approx \epsilon_B/\epsilon_e) = 1.1 \times 10^{-2}$. Note that this parameter set is the same one as used in Ref. [64] and it does not allow for accelerating cosmic rays up to ultra-high energies.

(1 + z)) as

$$\begin{aligned} 0.5Z^{-1}\eta\Gamma_1 E_{N,20} &\lesssim L_{M,48}^{1/2}\epsilon_{B,-1}^{1/2}\left(\frac{\Gamma_{\text{sh}}(\Gamma_{\text{sh}}-1)}{2}\right)^{1/2} \\ &\lesssim 0.55A^4Z^{-3}\eta^{-1}r_{15}\Gamma_1^3E_{N,20}^{-2}, \quad (\text{A3}) \end{aligned}$$

which is the same as Eq. (2) of Ref. [14]. As seen from the above inequalities, acceleration of protons above $\sim 10^{20}$ eV in LL GRBs will be more difficult than that in HL GRBs, because necessary parameters should be suitably chosen. For protons to be accelerated above $\sim 10^{20}$ eV, relatively more luminous/magnetized LL-GRBs with higher Lorentz factors are required. In fact, GRB 031203, whose redshift and luminosity are intermediate between two dim events (GRB 060218 and GRB 980425) and usual HL GRBs, might be such an event [11, 97]. Eqs. (A1) and (A2) just mean that UHECR production is also possible in relatively lower luminous GRBs such as XRFs and LL GRBs, even if LL GRBs do not form a distinct population.

In Fig. 3, we have shown the results in cases where acceleration and survival of UHE nuclei are possible. For comparison, we show the results for the parameter set used in Ref. [14]. In this case, the collision radius is smaller, so that we cannot expect survival of UHE nuclei. Protons can be accelerated up to $\sim 5 \times 10^{19}$ eV while Fe nuclei up to $\sim 10^{20}$ eV (but photodisintegrated).

In Fig. 5, we show the results for parameters inferred by Ghisellini et al. [64]. A collision radius is small enough, $r = 7 \times 10^{12}$ cm, so that the photomeson production and photodisintegration efficiencies are rather high. Because the photodisintegration and photomeson production processes prohibit acceleration of cosmic rays up to very high-energy, we cannot even expect UHECR production in this case.

APPENDIX B: ENERGETICS OF GRBS AND UHECRS

In this section, let us briefly overview the energetics of GRBs and UHECRs in order to see that GRBs (and hypernovae) could be one of the candidates of UHECRs (despite of some caveats). The detailed arguments are found in Refs. [1, 2, 3, 7, 9, 22, 98, 99, 100, 101]. In the previous section, we have seen that relativistic outflows that make GRBs satisfy various conditions for cosmic rays to be accelerated up to greater than 10^{20} eV. Here, let us compare the energy generation rate of observed UHECRs with the gamma-ray energy generation rate of GRBs. The UHECR generation rate given by Ref. [101] from Fly's Eye data is $E_{\text{CR}}^2 d\dot{N}_{\text{CR}}/dE_{\text{CR}} \approx 0.65 \times 10^{44}$ ergs Mpc $^{-3}$ yr $^{-1}$. The UHECR generation rate from the recent PAO results [102] is compiled by Dermer [22]. The UHECR generation rate at 10^{19} eV is $E_{\text{CR}}^2 d\dot{N}_{\text{CR}}/dE_{\text{CR}} \approx 0.8 \times 10^{44}$ ergs Mpc $^{-3}$ yr $^{-1}$. At higher energies, the value becomes smaller.

The radiation energy generation rate of GRBs is given by the product of the local GRB rate $\rho(0)$ (without the beaming-correction) and the average (isotropic equivalent) gamma-ray energy release E_{γ}^{iso} . First, let us consider HL GRBs. Recently, Kocevski & Butler [103] provided $E_{\gamma,[1\text{keV},10\text{MeV}]}^{\text{iso}} \sim (4.1 - 7.8) \times 10^{52}$ ergs, in a rest frame bandpass $(1 - 10^4)$ keV. Emission at higher energies (above the $(1 - 10^4)$ keV band) implies that the total gamma-ray energy input can be even higher. Assuming $\beta \sim 2$, we can expect $E_{\gamma}^{\text{iso}} \sim (1 - 2) \times 10^{53}$ ergs. The energy input at high energies is rather uncertain, because it depends on the high-energy photon index, pair-creation cutoff and possible inverse-Compton contribution. Here, we just adopt 2.5×10^{53} ergs as just a reference value for HL GRBs. On the other hand, by using logN-logS relationship with the assumption that the GRB rate traces, e.g., the star formation rate, various authors estimated the local GRB rate. In the pre-Swift era, the estimated long GRB rate was $\sim (0.2 - 1)$ Gpc $^{-3}$ yr $^{-1}$ (see, e.g., [13] and references there in). After the launch of *Swift*, many GRBs including high-redshift bursts were observed, and various authors provided the local GRB rate (see, e.g., [4, 5]). For example, Ref. [5] obtained $(0.2 - 0.3)$ Gpc $^{-3}$ yr $^{-1}$ assuming that the GRB rate traces the star formation rate. However, some authors claimed that the GRB rate has a faster evolution with redshift, which leads to the lower local GRB rate, ~ 0.05 Gpc $^{-3}$ yr $^{-1}$ [4, 5, 6]. Next, we shall consider LL GRBs. However, the radiation energy release and local rate of LL GRBs are much more uncertain. The radiation energy of GRB 060218 is $\sim 10^{50}$ ergs, while that of GRB 980425 is an order of magnitude smaller. The suggested local LL GRB rate is $\sim 10^{2-3}$ Gpc $^{-3}$ yr $^{-1}$ which are likely to be much higher than the local HL GRB rate [11, 12]. Note that we cannot exclude possibilities that there is no such a distinct population, although we assume the existence of LL GRBs in this paper. Too large rates might also be impossible due to constraints from observations of SNe Ibc. For example, Soderberg et al. [104] argued that at most $\sim 10\%$ of SNe Ibc are associated with off-beam GRBs based on their late-time radio observations of 68 local SNe Ibc.

Now, we can estimate the UHECR generation rate of GRBs from the radiation energy generation rate with an unknown baryon loading factor, which is defined by $U_{\text{CR}} \equiv \xi_{\text{acc}} U_{\gamma}$. Then, the cosmic-ray energy generation rate of GRBs can be written as $\mathcal{E}_{\text{CR}}^{\text{iso}} = \xi_{\text{acc}} E_{\gamma}^{\text{iso}} = \xi_{\text{acc}} (4\pi r^2 l) \Gamma U_{\gamma} N$. Here, let us introduce R which is defined as $R^{-1} \equiv (E_{\text{CR}}^2 \frac{d\dot{N}_{\text{CR}}}{dE_{\text{CR}}}) / \mathcal{E}_{\text{CR}}$, where $E_{\text{CR}}^2 \frac{d\dot{N}_{\text{CR}}}{dE_{\text{CR}}}$ is the cosmic-ray energy input at $10^{18.5-19.5}$ eV. When we assume $p = 2$ as the source spectral index of UHECRs, we have $R \equiv \ln(E_{\text{CR}}^{\text{max}}/E_{\text{CR}}^{\text{min}})$. The minimum energy is not well determined theoretically, but we can expect $E_N^{\text{min}} \sim \text{a few} \times \Gamma m_N c^2 \sim 10^{11.5}$ eV. We have also assumed that cosmic rays can be accelerated up to ultra-high energies, so that we can take $E_N^{\text{max}} \gtrsim 10^{20}$ eV. Hence, for HL-

GRBs, we obtain [105]

$$E_{\text{CR}}^2 \frac{d\dot{N}_{\text{CR}}}{dE_{\text{CR}}} = 5.0 \times 10^{43} \text{ ergs Mpc}^{-3} \text{ yr}^{-1} \left(\frac{\xi_{\text{acc}}}{20} \right) \left(\frac{20}{R} \right) \times \left(\frac{E_{\gamma}^{\text{iso}}}{2.5 \times 10^{53} \text{ ergs}} \right) \left(\frac{\rho_{\text{HL}}(0)}{0.2 \text{ Gpc}^{-3} \text{ yr}^{-1}} \right) \quad (\text{B1})$$

and for LL GRBs,

$$E_{\text{CR}}^2 \frac{d\dot{N}_{\text{CR}}}{dE_{\text{CR}}} = 5.0 \times 10^{43} \text{ ergs Mpc}^{-3} \text{ yr}^{-1} \left(\frac{\xi_{\text{acc}}}{10} \right) \left(\frac{20}{R} \right) \times \left(\frac{E_{\gamma}^{\text{iso}}}{2 \times 10^{50} \text{ ergs}} \right) \left(\frac{\rho_{\text{LL}}(0)}{500 \text{ Gpc}^{-3} \text{ yr}^{-1}} \right) \quad (\text{B2})$$

Therefore, the UHECR energy generation rate is roughly comparable to the radiation energy generation rate of GRBs (unless, for example, we use the smaller local GRB rate inferred from the faster evolution with redshift).

In other words, we can expect $E_{\text{CR}}^2 \frac{d\dot{N}_{\text{CR}}}{dE_{\text{CR}}}(10^{19} \text{ eV}) \sim \epsilon_{\text{ob}}^2 \frac{d\dot{N}_{\gamma}}{d\epsilon_{\text{ob}}}(\epsilon_{\text{ob}}^b)$ for both of HL GRBs and LL GRBs, and two populations can supply the necessary amount of UHECRs, when $\xi_{\text{acc}} \sim 10$ and $p \sim 2$. From Eq. (B1), we may have the required baryon loading factor $\xi_{\text{acc}} \gtrsim 20$ for HL GRBs, which is consistent with Ref. [22]. (If the local HL GRB rate is very low, as recently suggested by some authors, very large baryon loading factors $\xi_{\text{acc}} \gtrsim 100$ will be required, which would be implausible [8]). However, its value is not so solid and smaller ξ_{acc} could be possible, because the local GRB rate (and the total radiation energy input and the minimum cosmic-ray energy) is not much certain, and we may expect that GRB is one of the UHECR candidates at present.

In the reverse-forward and/or hypernova models, we usually use the kinetic energy of ejecta instead of the radiation energy of the prompt emission. The nonthermal cosmic-ray energy is written as $\mathcal{E}_{\text{CR}} \equiv \epsilon_{\text{acc}} E_{\text{ej}}$. In the case of supernova, $\epsilon_{\text{acc}} \gtrsim 0.1$ is typically needed to explain the cosmic-ray flux below the knee. From observations of afterglows, we typically have $E_{\text{ej}} \sim 10^{52-53}$ ergs for HL GRBs, while $E_{\text{ej}} \sim 10^{50-51}$ ergs for LL GRBs. In the hypernova model, the total kinetic energy of the hypernova ejecta, $E_{\text{ej}} \sim 5 \times 10^{52}$ ergs is expected (see [16] and references there in). But note that UHECRs can be produced only in the high velocity ejecta with $\Gamma\beta \gtrsim 0.5$, which carries $E_{\text{ej}} \sim 2 \times 10^{51}$ ergs [16, 17]. For these models, instead of Eq. (B2), we have

$$E_{\text{CR}}^2 \frac{d\dot{N}_{\text{CR}}}{dE_{\text{CR}}} = 4.0 \times 10^{43} \text{ ergs Mpc}^{-3} \text{ yr}^{-1} \epsilon_{\text{acc}} \left(\frac{25}{R} \right) \times \left(\frac{E_{\text{ej}}^{\text{iso}}}{2 \times 10^{51} \text{ ergs}} \right) \left(\frac{\rho_{\text{LL}}(0)}{500 \text{ Gpc}^{-3} \text{ yr}^{-1}} \right) \quad (\text{B3})$$

Hence, UHECRs could be explained in the external shock model and/or hypernova model for LL GRBs as well as the external shock model for HL GRBs. A significant

fraction of the kinetic energy must be injected to the non-thermal cosmic-ray energy. As in the case of supernovae, $\epsilon_{\text{acc}} \sim 0.1 - 1$ will be required. Note that the hypernova model is originally considered in order to explain high-energy cosmic rays above the second knee, where the cosmic-ray spectrum is formed by the superposition of cosmic-rays from hypernova ejecta with various velocities. The velocity profile with $dE_{\text{ej}}/d(\Gamma\beta) \propto (\Gamma\beta)^{-3}$ leads to the superposed spectral index $p \sim 3$ (which seems too steeper than the typical values of the required source spectrum index around the second knee for protons, $p \sim 2.4 - 2.7$). In order to explain UHECRs above the ankle only by the hypernova model, we would need some additional reason (which was not given in Refs. [16, 17]), such as, e.g., the variable index of the velocity profile or the velocity-dependent baryon loading. Instead, the hybrid model (GRBs and hypernovae) might be possible.

The above estimates are based on the assumption that the source spectral index is $p = 2.0$. However, if it is steeper, the required energy generation rate becomes much larger. In the dip model suggested by [9, 10], the typical spectral index is $p \sim 2.4 - 2.7$, which is steeper than $p \sim 2.0 - 2.3$ in the ankle model. Such a steep spectrum leads to the larger baryon loading factor, unless we change $E_{\text{CR}}^{\text{min}}$. For example, we have $R(10^{19} \text{ eV}) \equiv \mathcal{E}_{\text{CR}} / (E_{\text{CR}}^2 \frac{d\dot{N}_{\text{CR}}}{dE_{\text{CR}}}(10^{19} \text{ eV})) \sim 2500$ for $p = 2.4$ and $E_{\text{CR}}^{\text{min}} \sim 10^{11.5} \text{ eV}$, which can be obtained easily from its definition. Furthermore, we have neglected the cosmic-ray energy loss at the source. For example, the efficient neutrino production leads to depletion of high-energy cosmic rays if the shock dissipation at sufficiently inner radii. When $f_{p\gamma}$ is not small, the required nonthermal cosmic-ray energy will be raised by $\sim 1/(1 - f_{p\gamma})$. In addition, the adiabatic loss and escape of particles should be taken into account for more realistic calculations.

From Eqs. (B1), (B2) and (B3), we expect that GRBs can be the main UHECR sources in both of the internal shock model, and the external reverse and forward shock model. However, note that too large nonthermal baryon loading factors seem implausible because the available energy for nonthermal cosmic rays would be limited, e.g., by gravitational energy of falling materials of massive stars. In addition, the high radiative efficiency of the prompt emission [106] might infer that the large baryon loading is impossible, as long as the nonthermal baryon energy is smaller than the thermal baryon energy. Although these possible caveats, current theories cannot answer whether efficient UHECR production in GRBs is possible or not. Rather, we should test this GRB-hypothesis from observations. Current and future observations of UHECRs, neutrinos and gamma rays will give us useful information. For example, observations by AMANDA and IceCube have enabled us to constrain the averaged value of $f_{p\gamma}$ under the GRB-UHECR hypothesis [107, 108].

APPENDIX C: THE NEUTRINO BACKGROUND

It is very important to consider the neutrino background from GRBs since it is not easy to detect neutrino signals from one GRB event. The cumulative neutrino background flux from HL GRBs can be approximately evaluated by the following analytical expression using $R \sim 20$ [34, 89],

$$\begin{aligned} E_\nu^2 \Phi_\nu &\sim \frac{c}{4\pi H_0} \frac{1}{4} \min[1, f_{p\gamma}] E_p^2 \frac{dN_p^{\text{iso}}}{dE_p} \rho_{\text{HL}}(0) f_z \\ &\simeq 4 \times 10^{-9} \text{GeVcm}^{-2} \text{s}^{-1} \text{str}^{-1} \left(\frac{\xi_{\text{acc}}}{20} \right) E_{\gamma,53}^{\text{iso}} \\ &\times \left(\frac{f_{p\gamma}}{0.3} \right) \left(\frac{\rho_{\text{HL}}(0)}{0.2 \text{Gpc}^{-3} \text{yr}^{-1}} \right) \left(\frac{f_z}{3} \right), \quad (\text{C1}) \end{aligned}$$

and for LL GRBs we have [14]

$$\begin{aligned} E_\nu^2 \Phi_\nu &\sim \frac{c}{4\pi H_0} \frac{1}{4} \min[1, f_{p\gamma}] E_p^2 \frac{dN_p^{\text{iso}}}{dE_p} \rho_{\text{LL}}(0) f_z \\ &\simeq 7 \times 10^{-10} \text{GeVcm}^{-2} \text{s}^{-1} \text{str}^{-1} \left(\frac{\xi_{\text{acc}}}{10} \right) E_{\gamma,50}^{\text{iso}} \\ &\times \left(\frac{f_{p\gamma}}{0.05} \right) \left(\frac{\rho_{\text{LL}}(0)}{500 \text{Gpc}^{-3} \text{yr}^{-1}} \right) \left(\frac{f_z}{3} \right), \quad (\text{C2}) \end{aligned}$$

where f_z is the correction factor for the possible contribution from high redshift sources, which depends on the cosmology. In this paper, we use the standard Λ CDM cosmology with $\Omega_m = 0.3, \Omega_\Lambda = 0.7; H_0 = 71 \text{km s}^{-1} \text{Mpc}^{-1}$.

In general, we have to care about other backgrounds such as the atmospheric neutrino background when we consider the neutrino background. Observations of neutrinos from GRBs have merits that we can take the time- and positional-coincidence. Since HL GRBs are bright in the gamma-ray energy range, we expect the coincidence between neutrinos and gamma rays, which enables us to neglect the atmospheric and cosmogenic neutrino background essentially. On the other hand, neutrino signals from LL-GRBs are very dim in the sense that most of the neutrino signals will not correlate with photon signals. Only for very nearby bursts, we might be able to expect such correlations, and that it requires many-years operations. However, we may see neutrino events that are positionally correlated with SNe Ic associated with LL GRBs. The angular resolution of IceCube for neutrinos is about 1 degree or so, which might be searched by the optical-infrared follow-ups with ground-based optical telescopes [14]. Of course, it is necessary that the LL GRB neutrino background makes the dominant contribution to the neutrino background in this case.

Note that the GRB-UHECR hypothesis might lead to the enhanced cosmogenic neutrino background. Cosmogenic neutrinos are generated when UHECRs propagate in the universe, and they are the most promising very high-energy neutrino signals. Recent studies have suggested that GRBs may have the strong evolution with

redshifts, so that UHECR sources have the strong evolution if they are GRBs. In general, the strong evolution of UHECR sources leads to the higher cosmogenic neutrino background flux, which may be useful as one of the indirect clues to the GRB-UHECR hypothesis [109]. In addition, these neutrino signals can give us information on the source spectral index, that is, they are useful to distinguish between the ankle model and the dip model [110, 111].

APPENDIX D: HIGH-ENERGY NEUTRINOS AND GAMMA RAYS IN THE REVERSE-FORWARD SHOCK MODEL

In the reverse-forward shock model as well as the internal shock model, neutrino signals are expected. The neutrino emission in the early afterglow phase was studied in detail in Refs. [35, 50]. We can evaluate the photomeson production efficiency as [35]

$$f_{p\gamma} \simeq 0.088 \frac{L_{b,48}}{r_{16} \Gamma_2^2 \varepsilon_{\text{ob},10\text{eV}}^b} \begin{cases} (E_p/E_p^b)^{\beta-1} & (E_p < E_p^b) \\ (E_p/E_p^b)^{\alpha-1} & (E_p > E_p^b) \end{cases} \quad (\text{D1})$$

where $\varepsilon_{\text{ob}}^b$ is $\varepsilon_{\text{ob}}^m$ or $\varepsilon_{\text{ob}}^c$ or $\varepsilon_{\text{ob}}^{sa}$. In the reverse-forward shock model, we typically obtain $f_{p\gamma} < 1$ except in the highest energies. The typical neutrino energy is around $\sim 10^{18}$ eV rather than $\sim 10^{15}$ eV (which is expected for the prompt emission). Hence, expected muon event rates by IceCube are generally small, and the detection is not so easy even by other detectors such as PAO. Nevertheless, since EeV neutrinos are produced by $\sim 10^{20}$ eV protons, the detection of such very high-energy neutrinos is useful for diagnosing UHECR acceleration at acceleration sites. (For the prompt emission, the typical neutrino energy is $\sim \text{PeV}$, and PeV neutrinos are produced by protons with $\sim 10^{17}$ eV, smaller than ultra high energies.)

Next, let us consider the forward shock model. From Eq. (D1) and various quantities derived under the forward shock model, we can obtain the photomeson production efficiency. By replacing ε^b and L_b with $\varepsilon_{\text{ob}}^c$ and $\Gamma^2(\varepsilon^c \varepsilon^m)^{1/2} L_{\varepsilon, \text{max}}$, respectively, we have

$$f_{p\gamma} \simeq 2.1 \times 10^{-2} g_{-1} \epsilon_{e,-1} \epsilon_{B,-1}^{3/2} E_{\text{ej},53} n_0^{3/2} \begin{cases} (E_p/E_p^b)^1 \\ (E_p/E_p^b)^{0.5} \end{cases} \quad (\text{D2})$$

As seen in the previous section, $f_{p\gamma}$ increases with time in the ISM case (before the jet break), while decreases in the wind-medium case. For example, when we assume $\epsilon_{\text{acc}} E_{\text{ej}} = 10^{54}$ ergs and $\rho_{\text{HL}}(0) = 0.2 \text{Gpc}^{-3} \text{yr}^{-1}$, the expected diffuse neutrino flux at the break energy $E_\nu^b \approx 0.05 E_p^b$ is $E_\nu^2 \Phi_\nu \sim 6 \times 10^{-11} g_{-1} \epsilon_{e,-1} \epsilon_{B,-1}^{3/2} E_{\text{ej},53} n_0^{3/2} (f_z/3) \text{GeVcm}^{-2} \text{s}^{-1} \text{sr}^{-1}$.

In the higher energies, $E_\nu^2 \Phi_\nu$ becomes larger.

In the cases where UHE nuclei can survive as demonstrated in Figs. 6 and 7, we have $f_{\text{Fe}\gamma} \lesssim 1$ at $E_{\text{Fe}} \sim 10^{20}$ eV. From Eq. (16), we obtain $f_{p\gamma} \lesssim 4 \times 10^{-3}$ at $E_p \sim$

10^{20} eV. Hence, we can estimate the cumulative background neutrino flux as $E_\nu^2 \Phi_\nu \lesssim 10^{-10} \text{ GeV cm}^{-2} \text{ s}^{-1} \text{ sr}^{-1}$ at $E_\nu \sim 10^{18}$ eV under the GRB-UHECR hypothesis.

High-energy gamma-ray emission from the reverse-forward shock model is expected as well as the internal shock model (see, e.g., [112, 113]). For example, let us consider the forward shock model. In deriving Eq. (19), let us replace ε^b , $\alpha = 1$ and $\beta = 2.2$ with ε^c , $\alpha = 1.5$ and $\beta = 2$ (for $p = 2$). As a result, the optical thickness for pair-creation at $\varepsilon_{\text{ob}} = 10^{12}$ eV $\varepsilon_{\text{ob},12}$ can be evaluated as

$$\frac{f_{\gamma\gamma}(\varepsilon_{\text{ob}} = 10^{12} \text{ eV})}{f_{N\gamma}(E_N = 10^{20} \text{ eV})} \simeq 0.025 \left(\frac{A}{56}\right)^{-0.815} \left(\frac{\varepsilon_{\text{ob},12}^2 \varepsilon_{\text{ob},2}^c}{E_{N,20} \Gamma_2^2}\right)^{0.5} \quad (\text{D3})$$

where we have assumed $\varepsilon_{\text{ob}} \lesssim \tilde{\varepsilon}_{\text{ob}}^c = \Gamma^2 (m_e c^2)^2 / \varepsilon_{\text{ob}}^c$ and $E_N > E_N^b$, which can be realized at $t \sim 10^2$ s. At later time, we can expect $\varepsilon_{\text{ob}} \sim 10^{12}$ eV $\gtrsim \tilde{\varepsilon}_{\text{ob}}^c$ and have

$$\frac{f_{\gamma\gamma}(\varepsilon_{\text{ob}} = 10^{12} \text{ eV})}{f_{N\gamma}(E_N = 10^{20} \text{ eV})} \simeq 0.27 \left(\frac{A}{56}\right)^{-0.815} \left(\frac{\varepsilon_{\text{ob},12}}{E_{N,20}}\right)^{0.5} \quad (\text{D4})$$

Hence, we can expect that \sim TeV gamma rays escape from the source when UHE irons can survive. In fact, we typically expect such cases in the afterglow phase [112, 113]. Knowing the possible intrinsic pair-creation cutoff in the afterglow emission might give us clues to whether UHE heavy nuclei can survive or not. However, it may be difficult to distinguish the intrinsic pair-creation cutoff from other possibilities such as that due to attenuation by CMB/CIB photons and that due to the maximum accelerated energy of electrons.

APPENDIX E: HIGH-ENERGY NEUTRINOS AND GAMMA RAYS IN THE HYPERNOVA MODEL

In the hypernova model, not only nonthermal photons radiated from relativistic electrons but also thermal photons (in the optical band) exist at the relatively early time. High-energy neutrino emission generated via photomeson production is expected, but the detection would be difficult [16]. Instead, high-energy gamma rays may be detected by GLAST and/or MAGIC in the future. We can show that the optical depth against these thermal photons will be smaller than the unity. Although photon spectra of hypernovae are very complicated, let us make the very simple estimation by using a black-body spectrum. We have

$$f_{\gamma\gamma}(\varepsilon_{\text{ob}}) \sim 0.35 \left(\frac{kT}{1 \text{ eV}}\right) \left(\frac{r}{1 \text{ pc}}\right) \left(\frac{\varepsilon_{\text{ob}}}{1 \text{ PeV}}\right)^{-2}. \quad (\text{E1})$$

Therefore, hadronic gamma rays from high-energy neutral pions, muons and pairs above \sim PeV could escape from the source. They will be cascaded by CMB/CIB photons. After our work was public, Asano & Mészáros performed detailed calculations, and they also showed

that high-energy gamma rays can escape from the source [85]. They demonstrated that not only gamma rays from cosmic-ray synchrotron radiation but also secondary gamma rays generated via pair-creation by the CMB/CIB photons can be detected in the future, if the intergalactic magnetic field is weak enough.

APPENDIX F: GRBS AND UHECR ASTRONOMY

The discussions toward UHECR astronomy have been recently begun. The direct correlation between UHECR sources and observed UHECR arrival directions is one of the approaches to study the source properties. This can be expected only if the deflection angle due to the galactic magnetic field (GMF) and EGMF is small enough. The latter is poorly known both theoretically and observationally. $\sim (40 - 95)\%$ of volume within 100 Mpc can be regarded as the void region, whose uniform magnetic field is not well-known. The Faraday rotation measurement of radio signals from distant quasars implies $B_{\text{EG}}^{\text{void}} \lambda_{\text{Mpc}}^{1/2} \lesssim 10^{-9} \text{ GMpc}^{1/2}$ [114, 115]. In addition, there is also the structured EGMF which traces the local matter distribution. Observationally, clusters of galaxies have strong magnetic fields with $(0.1 - 1) \mu\text{G}$ at its center. This structured EGMF is very important for UHECR propagation (see, e.g., [116, 117] and references therein). The GMF is relatively well measured, but the magnetic field of the galactic halo is not known well. This GMF also affects trajectories of UHECRs [118]. If UHECR trajectories are deflected only weakly, the deflection angle by EGMF can be written as

$$\theta_d \approx \frac{\sqrt{2} Z e B_{\text{EG}} D}{3 E_N \sqrt{D/\lambda}} \simeq 2.5^\circ Z_1 E_{N,20}^{-1} B_{\text{EG},-10} \lambda_{\text{Mpc}}^{1/2} D_{100 \text{ Mpc}}^{1/2} \quad (\text{F1})$$

$$\theta_d \approx \frac{Z e B_{\text{EG}} D}{2 E_N} \simeq 2.6^\circ Z_1 E_{N,20}^{-1} B_{\text{EG},-11} D_{100 \text{ Mpc}}. \quad (\text{F2})$$

Eq. (F2) is for the coherent EGMF ($\theta_d D \ll \lambda$), while Eq. (F1) is for the EGMF with the coherent length λ ($\theta_d D \gg \lambda$). Recent PAO results imply the $\sim 3^\circ$ deflection angle, assuming that nearby AGN are UHECR sources [20, 21]. The inferred value $B_{\text{EG}} \sim 10^{-10}$ G is consistent with the predicted EGMF strength, and it could be used to set lower limits on the effective EGMF [22]. However, in fact, we cannot neglect the effect of the GMF. Although the deflection angle due to the GMF depends on the model of the galactic magnetic field, it can become $\gtrsim 3^\circ$. Therefore, lower limits could be set only if we see the direction where the effect of the GMF is small. In addition, the inferred value is derived from the positional correlation between the arrival directions of UHECRs and the incomplete AGN catalogue used by the PAO collaboration. Therefore, in general, more ob-

servations and careful examinations are required in order to estimate the effective EGMF from correlation signals.

Although the GMF can be important for the deflection angle, it does not affect the delayed time so much. From Eqs. (F1) and (F2), we can estimate the delayed time of UHECRs as

$$\tau_d \approx \frac{D\theta_d^2}{4c} \simeq 10^3 \text{ yrs } Z^2 E_{N,20}^{-2} \times B_{\text{EG},-10}^2 \lambda_{\text{Mpc}} D_{100 \text{ Mpc}}^2 \quad (\text{F3})$$

$$\tau_d \approx \frac{D\theta_d^2}{2c} \simeq 3.5 \times 10^3 \text{ yrs } Z^2 E_{N,20}^{-2} \times B_{\text{EG},-11}^2 D_{100 \text{ Mpc}}^3. \quad (\text{F4})$$

Eq. (F4) is for the coherent EGMF, while Eq. (F3) is for the EGMF with coherent length λ . Later we shall use the former expression for convenience. Note that the EGMF in the above equations expresses the effective EGMF field. UHE protons suffer from the stochastic energy loss due to photomeson production above the GZK energy, so that the dispersion of the arrival time is also $\sim \tau_d$. As long as we can use Eq. (F3), we also expect multiplets such that the lower energy cosmic-ray event precede higher energy cosmic-ray event, because the time delay is statistically distributed [100].

From the delayed time and observed local GRB rate, we can estimate the number density of GRB-UHECR sources. Let us perform a simple analytic calculation for the number density of GRB-UHECR sources. Following Ref. [119], we adopt the top-hat model, where the effect of energy losses are approximately negligible when $D < D_c(E_{\text{CR}})$, and eliminating all cosmic rays coming from $D > D_c(E_{\text{CR}})$. Here, $D_c(E_{\text{CR}})$ is the effective cutoff distance. For example, we obtain $D_c(E_p = 10^{20} \text{ eV}) \approx 50 \text{ Mpc}$ when we define that $D_c(E_{\text{CR}})$ is the radius from which $1/e$ of cosmic rays can reach us (see, e.g., [121]). By assuming that we can observe GRB-UHECR sources only during the duration time which is comparable to the delayed time $\sim \tau_d$, we have

$$F_{\text{CR}} \approx \frac{1}{4\pi D^2 \tau_d} \frac{dN_{\text{CR}}}{dE_{\text{CR}}}, \quad (\text{F5})$$

where F_{CR} is the observed UHECR flux at a given energy. Most cosmic rays above the effective cutoff radius D_c cannot reach us. Hence, the minimum flux F_{CR}^c for a given $\frac{dN_{\text{CR}}}{dE_{\text{CR}}}$ is obtained by substituting D_c into D . We also have the corresponding delayed time τ_d^c . The number density of GRB-UHECR sources at UHE energies is calculated by integrating the differential source number density (the number of GRBs per unit observed UHECR flux) over the UHECR flux $F_{\text{CR}} \gtrsim F_{\text{CR}}^c$. As a result, we have $n_s \approx (3/5)\rho(0)\tau_d^c$. Note that, in the GRB-UHECR hypothesis, the number density of UHECR sources will depend on the observed energy because τ_d^c depends on the energy. The number density of GRB-UHECR sources

observed at $E_p = 10^{19.9} \text{ eV}$ becomes

$$n_s^{\text{HL}} \approx \frac{3}{5}\rho_{\text{HL}}(0)\tau_d^c \simeq 1.7 \times 10^{-5} \text{ Mpc}^{-3} B_{\text{EG},-9}^2 \lambda_{\text{Mpc}} \times \left(\frac{\rho_{\text{HL}}(0)}{0.2 \text{ Gpc}^{-3} \text{ yr}^{-1}} \right) \quad (\text{F6})$$

$$n_s^{\text{LL}} \approx \frac{3}{5}\rho_{\text{LL}}(0)\tau_d^c \simeq 4.2 \times 10^{-5} \text{ Mpc}^{-3} B_{\text{EG},-10}^2 \lambda_{100 \text{ kpc}} \times \left(\frac{\rho_{\text{LL}}(0)}{500 \text{ Gpc}^{-3} \text{ yr}^{-1}} \right). \quad (\text{F7})$$

The number density of UHECR sources for arbitrary energies can be obtained by calculating D_c^2/E_{CR}^2 . Eqs. (F6) and (F7) suggest that determination of the number density of UHECR sources and effective EGMF enable us to test the GRB-UHECR hypothesis. Acquiring the latter is especially not easy, hence one of the ultimate goals of the UHECR astronomy. But future observations of UHECRs by PAO and TA will give us clues to them via observations of correlation signals.

The source number density can be estimated from the study of the small-scale anisotropy. If the observed small-scale clustering originates in the same sources, we can estimate the minimum number density of UHECR sources [122, 123]. For example, recent PAO observations showed 6 pairs with separation smaller than the correlation angle scale of 6° among the 27 highest-energy events. This leads to a lower limit for the number of sources ≥ 61 [21]. When we adopt $D_c \approx 130 \text{ Mpc}$, we can estimate the source number density as $n_s \gtrsim 3 \times 10^{-5} \text{ Mpc}^{-3}$. In more detail, the significance of small-scale clustering in the arrival directions of UHECRs can be studied by the angular two-point auto-correlation function. By simulating the arrival distribution of UHECRs, the source number density that can reproduce observational results can be estimated [124]. The constraint obtained from the small-scale anisotropy observed by AGASA is $n_s \gtrsim 10^{-5} \text{ Mpc}^{-3}$ for uniformly distributed proton sources. Despite large uncertainties due to a small number of observed events, PAO observations in the future can lead to the more robust estimation [125].

For example, if we can find that the source number density is $n_s \sim 10^{-4} \text{ Mpc}^{-3}$, the required effective EGMF for a given local GRB rate is $B_{\text{EG},-9}^2 \lambda_{\text{Mpc}} \sim 10$ (which might be larger the upper limit of the uniform EGMF) for HL GRBs and $B_{\text{EG},-9}^2 \lambda_{\text{Mpc}} \sim 0.005$ for LL GRBs. However, since the robust estimation of the source number density may be difficult, we may have only the lower limit. In such cases, for example, $n_s \gtrsim 10^{-5} \text{ Mpc}^{-3}$ would infer the required EGMF $B_{\text{EG},-9}^2 \lambda_{\text{Mpc}} \gtrsim 1$ for HL GRBs and $B_{\text{EG},-9}^2 \lambda_{\text{Mpc}} \gtrsim 0.0005$ for LL GRBs. Therefore, determination of the upper limit on the effective EGMF is important in order to test the GRB-UHECR hypothesis. If we know that the effective EGMF is too weak, possibilities of HL GRBs as observed main UHECR sources could be excluded. (However, we could still expect to see HL GRBs as rare but very bright UHECR sources. In such cases, one HL GRBs could be found

as a very bright event among $\sim \rho_{\text{LL}}(0)/\rho_{\text{HL}}(0) \sim 1000$ LLGRB-UHECR sources.) On the other hand, when the effective EGMF is strong enough, HL GRBs rather than LL GRBs would be more plausible main UHECR sources. It is because the too large source number density cannot explain the anisotropy [125]. Of course, when LL GRBs can also produce UHECRs, they could be regarded as numerous faint sources, and it is difficult to exclude the existence of such faint sources. More generally, we should employ the luminosity-weighted distribution rather than the luminosity-uniform distribution. Even if LL GRBs do not form a distinct population, it would be important to know the local GRB rate as a function of E_{γ}^{iso} for more refined investigations.

Although Eqs. (F6) and (F7) suggest that future observations enable us to test the GRB-UHECR hypothesis, the above estimation is simple and not quantitative. In order to present realistic arguments, we need the detailed simulation of cosmic-ray propagation, which is being planned as our future work. Note that, when UHECRs contain heavier nuclei, τ_d^c for heavy nuclei differs from that for protons, so that the source number density also depends on the composition of UHECRs.

Before finishing this section, let us briefly describe observable features which are expected for GRB-UHECR sources. In the GRB-UHECR model, we can expect several prominent features different from those in the steady source models. One can be observed in the clustering properties. Since the UHECR flux is proportional to D^{-4} as seen in Eq. (F5), the differential source number density is proportional to $F_{\text{CR}}^{-9/4}$ as long as we assume the

luminosity-uniform source distribution [119]. This leads to the source number density above F_{CR} is proportional to $F_{\text{CR}}^{-5/4}$, which differs from the steady source model where we have $\propto F_{\text{CR}}^{-3/2}$. This difference leads to the difference in the average number of multiplets, i.e., the difference in the ratio of the expected number of clusters with different multiplicities [123]. In the GRB-UHECR model, we may obtain the ratio between the number of triplets or higher multiplets and doublets, which is ~ 0.6 in the GRB-UHECR model, while ~ 0.33 in the steady source model.

Another prominent feature is the existence of the critical energy [119]. As seen in Eqs. (F6) and (F7), the source number density decreases with the energy. Since D_c decreases rapidly above the pion production threshold energy, τ_d^c will also show the rapid decrease above the pion threshold energy. Therefore, there exists the critical energy where the observed source number becomes the unity. Around this critical energy, we have possibilities to see the considerably higher flux than time-averaged UHECR flux from all sources. For the source number density $n_s = 10^{-5} \text{ Mpc}^{-3}$, we expect $E_c \sim 1.4 \times 10^{20} \text{ eV}$ for proton sources. For $n_s = 10^{-4} \text{ Mpc}^{-3}$, $E_c \sim 2.5 \times 10^{20} \text{ eV}$ is expected.

Note that, although we consider the extreme case where each population has the typical UHECR luminosity respectively, there are not necessarily clear differences between the two populations. For more detailed studies, we should take into account the distribution of the UHECR luminosity (i.e., luminosity-weighted model).

-
- [1] E. Waxman, Phys. Rev. Lett., 75, 386 (1995)
 - [2] M. Milgrom and V. Ussov, ApJ, 449, L37 (1995)
 - [3] M. Vietri, ApJ, 453, 883 (1995)
 - [4] T. Le and C.D. Dermer, ApJ, 661, 394 (2007)
 - [5] D. Guetta and T. Piran, JCAP, 07003 (2007)
 - [6] M.D. Kistler, H. Yuksel, J. Beacom, and K.Z. Stanek, ApJ, 673, L119 (2008)
 - [7] S.D. Wick et al., Astropart. Phys., 21, 125 (2004)
 - [8] K. Murase and S. Nagataki, Phys. Rev. D, 73, 063002 (2006)
 - [9] V. Berezhinsky, A.Z. Gazizov, and S.I. Grigorieva, PRD, 74, 043005 (2006)
 - [10] R. Aloisio et al., Astropart. Phys., 27, 76 (2007)
 - [11] D. Guetta and M.D. Valle, ApJ, 657, L73 (2007)
 - [12] E. Liang et al., ApJ, 670, 565 (2007)
 - [13] D. Guetta et al., ApJ, 615, L73 (2004)
 - [14] K. Murase, K. Ioka, S. Nagataki, and T. Nakamura, ApJ, 651, L5 (2006)
 - [15] N. Gupta and B. Zhang, Astropart. Phys., 27, 386 (2007)
 - [16] X.Y. Wang, S. Razzaque, P. Mészáros, and Z.G. Dai, Phys. Rev. D, 76, 083009 (2007)
 - [17] X.Y. Wang et al., arXiv:0711.2065
 - [18] K. Greisen, Phys. Rev. Lett. 16, 748 (1966)
 - [19] G.T. Zatsepin and V.A. Kuz'min, Sov. Phys. JETP. Lett., 4, 78 (1966)
 - [20] Pierre Auger Collaboration, Science, 318, 938 (2007)
 - [21] Pierre Auger Collaboration, arXiv:0712.2843
 - [22] C.D. Dermer, arXiv:0711.2804 (2007)
 - [23] Pierre Auger Collaboration, arXiv:0706.1495
 - [24] D. Gorbunov et al., arXiv:0711.4060
 - [25] T. Wibig and A.W. Wolfendale, arXiv:0712.3403
 - [26] J. Ahrens et al., Astropart. Phys., 20, 507 (2004)
 - [27] U.F. Katz, Nucl. Instrum. Meth., A567, 457 (2006)
 - [28] S.W. Barwick et al., Phys. Rev. Lett., 96, 171101 (2006)
 - [29] V. Van Elewyck et al., astro-ph/0612731 (2006)
 - [30] E. Waxman and J. Bahcall, Phys. Rev. Lett., 78, 2292 (1997)
 - [31] E. Waxman and J. Bahcall, ApJ, 541, 707 (2000)
 - [32] Z.G. Dai and T. Lu, ApJ, 551, 249 (2001)
 - [33] C.D. Dermer, ApJ, 574, 65 (2002)
 - [34] K. Murase and S. Nagataki, Phys. Rev. Lett., 97, 051101 (2006)
 - [35] K. Murase, Phys. Rev. D, 76, 123001 (2007)
 - [36] K. Murase and K. Ioka, ApJ, 676, 1123 (2008)
 - [37] C.D. Dermer, E. Ramirez-Ruiz, and T. Le, ApJ, 664, L67 (2007)
 - [38] K. Murase, K. Asano, and S. Nagataki, ApJ, 671, 1886 (2007)
 - [39] T. Piran, Rev. Mod. Phys., 76, 1143 (2005)

- [40] P. Mészáros, Rep. Prog. Phys., 69, 2259 (2006)
- [41] B. Zhang, Chin. J. Astron. Astrophys., 7, 1 (2007)
- [42] R. Blandford and D. Eichler, Phys. Rep., 154, 1 (1987)
- [43] Note that expressions of $dn_{CR}/d\varepsilon_{CR}$ and $n_{\varepsilon, \max}$ in Ref. [35] included trivial typos. The expressions given in this paper is correct. Of course, all the results in Ref. [35] were calculated using the correct expressions.
- [44] U. Keshet and E. Waxman, Phys. Rev. Lett., 94, 111102 (2005)
- [45] M. Vietri, ApJ, 591, 954 (2003)
- [46] J. Aoi, K. Murase, and S. Nagataki, MNRAS, 383, 1431
- [47] J.P. Rachen and P. Mészáros, Phys. Rev. D, 58, 123005 (1998)
- [48] Y.A. Gallant and A. Achterberg, MNRAS, 305, L6 (1999)
- [49] A. Achterberg, Y.A. Gallant, J.G. Kirk, and A.W. Guthmann, MNRAS, 328, 393 (2001)
- [50] C.D. Dermer, ApJ, 664, 384 (2007)
- [51] Actually, the adiabatic loss and escape of cosmic rays should be taken into account carefully, because the cosmic-ray spectrum could be modified by these effects. Unfortunately, quantitative estimation is difficult and it is beyond the scope of this paper.
- [52] F.W. Stecker and M.H. Salamon, ApJ, 512, 521 (1999)
- [53] S. Agostinelli et al., Nuclear Instruments and Methods in Physics Research A, 506, 250-303 (2003), <http://wwwasd.web.cern.ch/wwwasd/geant4/geant4.html>
- [54] Particle Data Group, <http://pdg.lbl.gov/>
- [55] J.L. Puget, F.W. Stecker, and J.H. Bredekamp, ApJ, 205, 638 (1976)
- [56] S. Karakula and W. Tkaczyk, Astropart. Phys., 1, 229 (1993)
- [57] D. Allard et al., A&A, 443, L29 (2005)
- [58] K. Asano, ApJ, 623, 967 (2005)
- [59] K. Ioka, K. Murase, K. Toma, S. Nagataki, and T. Nakamura, ApJ, 670, L77 (2007)
- [60] S. Campana et al., Nature, 442, 1008
- [61] E. Waxman et al., ApJ, 667, 351 (2007)
- [62] X.Y. Wang et al., ApJ, 664, 1026 (2007)
- [63] Y.Z. Fan, T. Piran, and D. Xu, JCAP, 09013 (2006)
- [64] G. Ghisellini, G. Ghirlanda, and F. Tavecchio, MNRAS, 375, L36 (2007)
- [65] K. Toma et al., ApJ, 659, 1420 (2007)
- [66] P.W.A. Roming et al., ApJ, 652, 1416 (2006)
- [67] F. Genet, F. Daigne, and R. Mochkovitch, MNRAS, 381, 732 (2007)
- [68] L.Z. Uhm and A.M. Beloborodov, ApJ, 665, L93 (2007)
- [69] D. Eichler and E. Waxman, ApJ, 627, 861, (2005)
- [70] K. Toma, K. Ioka, and T. Nakamura, ApJ, 673, L123 (2008)
- [71] A.R. Bell, MNRAS, 353, 550 (2004)
- [72] M. Milosavljević and E. Nakar, ApJ, 641, 978 (2006)
- [73] C.D. Dermer and M. Humi, ApJ, 556, 479 (2001)
- [74] R. Wijers and T. Galama, ApJ, 523, 177 (1999)
- [75] The dependence on the composition can be seen especially when $f_{N\gamma} > 1$ [76].
- [76] L. A. Anchordoqui et al., Astropart. Phys., in press (2007)
- [77] C.D. Dermer and A. Atoyan, New. J. Phys. 8, 122 (2006)
- [78] K. Asano and S. Inoue, ApJ, 671, 645 (2007)
- [79] Too large baryon loading factors can change a seed photon spectrum below \sim GeV significantly, which may seem implausible. Hence, the baryon loading factor could be constrained from observations of high-energy gamma rays. However, note that the amount of hadronic gamma rays largely depends on $f_{p\gamma}$ when $f_{p\gamma} \lesssim 1$. This implies that the flux of proton-induced gamma rays is rather sensitive to the lower photon index α . Although there were some theoretical calculations [77, 78], the lower photon index is $\alpha \sim 1.5$ expected in fast cooling synchrotron spectra, rather than the typical value $\alpha \sim 1$. It can lead to the overestimation of hadronic gamma rays.
- [80] R. Svensson, MNRAS, 227, 403 (1987)
- [81] T. Kneiske et al., A&A, 413, 807 (2004)
- [82] http://www-glast.slac.stanford.edu/software/IS/glast_lat_performance.htm
- [83] J. Albert et al., ApJ, 667, 358 (2007)
- [84] E. Armengaud, G. Sigl, and F. Miniati, Phys. Rev. D, 73, 083008 (2006)
- [85] K. Asano and P. Mészáros, ApJ, 677, L31 (2008)
- [86] The intergalactic magnetic field is not necessarily the magnetic field in the structured region, which is expected to be relatively strong. In fact, the mean free path of TeV photons is a few \times Mpc, so that pairs can be generated in the void region whose magnetic field may be very weak. Note that UHECRs from sources in the structured region can be deflected only by the magnetic field in the structured region, even if we do not consider the magnetic field in the void region.
- [87] We do not take into account cosmogenic gamma rays produced during the UHECR propagation, which can also be expected if the intergalactic magnetic field is very weak [88].
- [88] E. Waxman and P. Coppi, ApJ, 464, L75 (1996)
- [89] E. Waxman and J. Bahcall, Phys. Rev. D, 59, 023002 (1998)
- [90] J. Pruet, S. Guiles, and G.M. Fuller, ApJ, 580, 368 (2002)
- [91] M. Lemoine, A&A, 390, L31 (2002)
- [92] S. Nagataki, A. Mizuta, S. Yamada, H. Takabe, and K. Sato, ApJ, 596, 401 (2003)
- [93] K. Maeda, K. Nomoto, ApJ, 598, 1163 (2003)
- [94] S. Nagataki, A. Mizuta, and K. Sato, ApJ, 647, 1255 (2006)
- [95] N. Tominaga, arXiv:0711.4815
- [96] W.Q. Zhang, S.E. Woosley, and S.E. MacFadyen, ApJ, 586, 356 (2003)
- [97] D. Malesani et al., ApJ, 609, L5 (2004)
- [98] S.T. Scully and F.W. Stecker, Astropart. Phys., 16, 271 (2002)
- [99] V. Berezhinsky, A.Z. Gazizov, and S.I. Grigorieva, hep-ph:0204357 (2002)
- [100] M. Vietri, D.D. Marco, and D. Guetta, ApJ, 592, 378 (2003)
- [101] E. Waxman, ApJ, 606, 988 (2004)
- [102] T. Yamamoto, for the Pierre Auger Collaboration, arXiv:0707.2638
- [103] D. Kocevski and N. Butler, arXiv:0707.4478
- [104] A.M. Soderberg et al., ApJ, 638, 930 (2006)
- [105] More precisely, in order to evaluate the total radiation energy rate, we have to take into account that the detection flux threshold is different among detectors.
- [106] K. Ioka et al., A&A, 458, 7 (2006)
- [107] A. Achterberg et al., ApJ, 664, 397 (2007)
- [108] A. Achterberg et al., ApJ, 674, 357 (2008)
- [109] H. Yuksel and M.D. Kistler, Phys. Rev. D, 75, 083004 (2007)

- [110] H. Takami, K. Murase, S. Nagataki, and K. Sato, arXiv:0704.0979
- [111] D. Allard et al., JCAP, 09005 (2006)
- [112] B. Zhang and P. Mészáros, ApJ, 559, 110 (2001)
- [113] Y.Z. Fan et al., MNRAS, 384, 1483 (2008)
- [114] P.P. Kronberg, Rep. Prog. Phys., 57, 325 (1994)
- [115] J.P. Vallée, New Astron. rev., 48, 763 (2004)
- [116] K. Dolag et al., JCAP 01009 (2005)
- [117] H. Takami and K. Sato, ApJ, 639, 803 (2006)
- [118] H. Takami and K. Sato, arXiv:0710.1434
- [119] J. Miralda-Escudé and E. Waxman, ApJ, 462, L59 (1996)
- [120] E. Waxman and J. Miralda-Escudé, ApJ, 472, L89 (1996)
- [121] D. Harari, S. Mollerach, and E. Roulet, JCAP, 11012 (2006)
- [122] S.L. Dubovsky, P.G. Tinyakov, and I.I. Tkachev, Phys. Rev. Lett., 85, 1154 (2000)
- [123] D. Harari, S. Mollerach, and E. Roulet, JCAP, 05010 (2004)
- [124] M. Kachelriess and D. Semikoz, Astropart. Phys., 23, 486 (2005)
- [125] H. Takami and K. Sato, Astropart. Phys., 28, 529 (2008)